Switchable Electrode Assemblies Employing Nano-Bio Hybrid Structures in Cascaded Enzymatic Fuel Cells

DISS. ETH NO. 24998

SWITCHABLE ELECTRODE ASSEMBLIES EMPLOYING NANO-BIO HYBRID STRUCTURES IN CASCADED ENZYMATIC FUEL CELLS

A thesis submitted to attain the degree of

DOCTOR OF SCIENCES of ETH ZURICH
(Dr. sc. ETH Zurich)

presented by
KATHARINA HERKENDELL

Dipl.-Ing., Karlsruher Institut für Technologie

born on 02.07.1987
citizen of Germany

accepted on the recommendation of

Prof. Dr. Andreas Stemmer, examiner
Prof. Dr. Marco Frasconi, co-examiner

2018

Abstract

Enzymatic biofuel cells may become more accessible for applications powering portable or implantable electronic devices by extending the range and conversion efficiency of the fuels and oxidizers used. One of the major challenges of enzyme-modified electrodes is their susceptibility to time-dependent degradation of the active biocatalysts, which typically leads to limited operational lifetimes.

Within this thesis, we introduce concepts and methodologies that promote enzymatic biofuel cells as alternative power sources. These concepts are exemplified and validated through a series of saccharide/oxygen-based enzymatic biofuel cells.

To broaden the spectrum of usable biofuels and operational conditions, we describe integrated assemblies consisting of multi-substrate electrodes composed of enzymatic cascades immobilized to mesoporous carbon nanoparticle supports. In this design, entrapped electron relay molecules facilitate the electrical communication between the linked redox enzymes and the conductive carbon supports, thus efficiently mediating the oxidation of multiple fuels and reduction of oxidizers for the generation of electrical power. By using a cascade consisting of the enzymes invertase, mutarotase, glucose oxidase and fructose dehydrogenase, and by employing tetrathiafulvalen mediator units, we are able to effectively oxidize, separately and simultaneously, the fuels glucose, fructose and sucrose. A cathode consisting of the enzymes catalase and bilirubin oxidase, employing the mediator 2,2'-azino-bis(3-ethylbenzothiazoline-6-sulfonic acid), is successfully shown to operate in environments of varied oxygen availability.

Whereas bilirubin oxidase reduces oxygen to water under aerobic conditions, catalase catalyzes the disproportionation reaction of hydrogen peroxide to water and oxygen, allowing hydrogen peroxide to act as an internal source of oxygen under anaerobic operation conditions. A combined assembly of these cascaded electrode architectures yields a non-compartmentalized biofuel cell based on mediated electron transfer bioelectrocatalysis, operating with multiple fuels and oxidizer resources. This cell can be repeatedly switched between aerobic and anaerobic operating conditions without any significant decrease in discharge performance.

To overcome limitations imposed by the time-dependent degradation of the biological components in enzymatic biofuel cells, we propose a magnetically assisted methodology to reenergize the cells. In this case, carbon coated magnetic nanoparticles are modified with fructose dehydrogenase or bilirubin oxidase. These can be channeled towards and away from designated current collectors by externally applied magnetic field gradients. The magneto-assisted loading of the current collectors results in direct electron transfer currents. Similarly, by applying appropriate magnetic field gradients, bioelectrocatalysis can be switched ON and OFF to generate power on demand, and the active components of the cell can be exchanged entirely to regenerate power. By repeatedly refreshing the particles at a deep stage of the discharge, the biofuel cell operation is considerably extended beyond a single full discharge. Taken individually and even more so when combined together, these concepts open new possibilities to exploit a broad range of fuels and oxidizers, and to harvest electrical energy from alternative biomass resources.

Zusammenfassung

Enzymatische Brennstoffzellen können für Anwendung in der Energieversorgung von tragbaren oder implantierbaren elektronischen Geräten zugänglicher gemacht werden, indem der Anwendungsbereich und die Umwandlungseffizienz der verwendeten Brennstoffe und Oxidationsmittel erweitert wird. Eine der größten Herausforderungen für enzymmodifizierte Elektroden ist ihre Empfindlichkeit gegenüber zeitbedingtem Abbau der aktiven Biokatalysatoren, was zu einer begrenzten Betriebsdauer führt.

In Rahmen dieser Arbeit stellen wir Konzepte und Methoden vor, die darauf abzielen, enzymatische Biobrennstoffzellen als alternative Energiequellen zu fördern. Diese Konzepte werden durch eine Reihe von Saccharid/Sauerstoff-basierten enzymatischen Biobrennstoffzellen veranschaulicht und validiert. Um das Spektrum verwendbarer Biokraftstoffe und möglicher Betriebsbedingungen zu erweitern, beschreiben wir die Zusammensetzung integrierter Multi-Substrat-Elektroden, die aus auf mesoporösen Kohlenstoffnanopartikeln immobilisierten enzymatischen Kaskaden bestehen. In diesem Design dienen eingeschlossene Mediatormoleküle zur elektrischen Kommunikation zwischen den immobilisierten Redoxenzymen und den leitfähigen Kohlenstoffträgern, wodurch die Oxidation von mehreren Brennstoffen und die Reduktion von Oxidationsmitteln für die Erzeugung von elektrischer Energie ermöglicht werden. Mit Hilfe einer Kaskade bestehend aus den Enzymen Invertase, Mutarotase, Glucose Oxidase und Fructose Dehydrogenase und unter Verwendung von Tetrathiafulvalen als Mediatormolekül können wir die Treibstoffe Glucose, Fructose und Saccharose getrennt

und gleichzeitig effektiv oxidieren. Es wird erfolgreich gezeigt, dass eine aus den Enzymen Katalase und Bilirubinoxidase bestehende Kathode unter Verwendung des Mediators 2,2′-Azino-di-(3-ethylbenzthiazolin-6-sulfonsäure) in Milieus mit variierender Sauerstoffverfügbarkeit arbeitet. Während Bilirubinoxidase unter aeroben Bedingungen Sauerstoff zu Wasser reduziert, katalysiert Katalase die Disproportionierungsreaktion von Wasserstoffperoxid zu Wasser und Sauerstoff, wodurch Wasserstoffperoxid als eine interne Sauerstoffquelle unter anaeroben Bedingungen dienen kann. Eine kombinierte Anordnung dieser kaskadierten Elektrodenarchitekturen ergibt eine membranlose Biobrennstoffzelle basierend auf mediiertem Elektronentransfer, die mit mehreren Brennstoffen und Oxidationsmittelressourcen arbeitet. Diese Brennstoffzelle kann wiederholt zwischen aeroben und anaeroben Betriebsbedingungen umgeschaltet werden, ohne dass die Leistung signifikant abnimmt.
Um die Einschränkungen durch den zeitbedingten Abbau der biologischen Komponenten in enzymatischen Biobrennstoffzellen zu überwinden, schlagen wir eine magnetisch unterstützte Methode vor um die Brennstoffzellen zu revitalisieren. In diesem Fall werden kohlenstoffbeschichtete magnetische Nanopartikel mit Fructose Dehydrogenase oder Bilirubin Oxidase modifiziert. Diese können durch extern angelegte Magnetfeldgradienten zu Stromabnehmern hin und von diesen weg geführt werden. Die magnetisch unterstützte Beladung der Stromkollektoren führt zu direkten Elektronentransferströmen durch die besagten Enzyme. In ähnlicher Weise kann durch Anlegen geeigneter Magnetfeldgradienten die Bioelektrokatalyse ein- und ausgeschaltet werden, um bei Bedarf Leistung abzurufen, oder die aktiven Komponenten der Zelle können vollständig ausgetauscht werden, um die Leistung zu regenerieren. Durch wiederholtes

Auffrischen der Partikel in einem tiefen Stadium der Entladung wird die Betriebsdauer der Biobrennstoffzelle beträchtlich über eine einzelne vollständige Entladung hinaus verlängert. Für sich und vor allem in Kombination eröffnen diese Konzepte neue Möglichkeiten um eine breite Palette an Brennstoffen und Oxidationsmitteln zu nutzen und elektrische Energie aus alternativen Biomassequellen zu gewinnen.

Acknowledgements

This thesis was conducted with various forms of support from family members, friends, colleagues and advisors. I am deeply grateful and would like to individually thank:

- Prof. Dr. Andreas Stemmer for supervising my doctoral thesis, for the provided opportunities and facilities, and for his guidance and support.
- Prof. Dr. Marco Frasconi for co-examining the thesis.
- Dr. Ran Tel-Vered for his guidance and support throughout the thesis.
- Alexander Trifonov for his practical support in the laboratory.
- Blerim Veselaj for technical and various other support.
- Dr. Tino Wagner and all current and former members of the Nanotechnology Group for the collegial atmosphere and support in multiple disciplines.

Contents

Abbreviations

ABTS	2,2′-azino-bis(3-ethylbenzothiazoline-6-sulfonic acid)
BOD	Bilirubin oxidase from *Myrothecium verrucaria*
BS^3	Suberic acid bis(3-sulfo-N-hydroxysuccinimide ester)
CAT	Catalase from bovine liver
ccMNP	Carbon coated magnetic nanoparticle
CE	Counter electrode
CV	Cyclic voltammogram
DET	Direct electron transfer
EBFC	Enzymatic biofuel cell
FAD	Flavin adenine dinucleotide
FcM	Ferrocene methanol
FDH	D-Fructose dehydrogenase from *Gluconobacter sp.*
GC	Glassy carbon
GOX	Glucose oxidase from *Aspergillus niger*
HEPES	4-(2-hydroxyethyl)-1-piperazineethanesulfonic acid
HRP	Peroxidase from horseradish
INV	Invertase *from Saccharomyces cerevisiae*
ITO	Indium tin oxide
LAC	Laccase from *Trametes versicolor*
$M_{1,2}$	Permanent magnet
mCNP	Mesoporous carbon nanoparticle
Me, Me^+	Mediator unit in reduced or oxidized state
MES	2-(N-morpholino)ethanesulfonic acid
MET	Mediated electron transfer
MNP	Magnetic nanoparticle
MUT	Mutarotase from porcine

NMP	N-methyl-2-pyrrolidone
OCP	Open circuit potential
PVDF	Polyvinylidene fluoride
RE	Reference electrode
SCE	Saturated Calomel Electrode
T1, T2, T3	Types of copper centers in multi-copper oxidases
TTF	Tetrathiafulvalene
WE	Working electrode

1 Introduction

The development of bioelectrochemical devices, such as biologically modified fuel cells or biosensors, constitutes a fast evolving area of research. A global effort is made to understand, mimic, and apply biological pathways of energy conversion in areas like medicine, environmental sciences, or electrical power generation and storage.[1,2]
Enzyme-based fuel cells facilitate electrical power generation from versatile biomass substrates. An enzymatic bioelectrochemical cell consists of two electrodes, at least one of which is enzyme-modified, where the anode catalyzes the oxidation of the fuel and the cathode catalyzes the reduction of the oxidizer. The concurrent oxidation and reduction processes at the electrodes yield electrical power, given a potential difference between the reactions. The enzymatic conversion of a substrate is highly selective and typically takes place under mild conditions regarding temperature and pH. This makes such processes attractive for electrical power generation in complex media and for driving medical implants under physiological conditions.[3-5] A major challenge in the field of bioelectrochemical energy conversion lies in enhancing the performance of biofuel cells in terms of power output and device lifetime. A milestone for biofuel cell fabrication was set, when the first non-compartmentalized biofuel cell was introduced.[6] Improved wiring methods associated with significantly improved electron transfer rates enabled the assembly of oxygen insensitive anodes employing naturally oxygen sensitive oxidoreductases like glucose oxidase (GOX). The obsolescence of a separating membrane between anodic and cathodic half-cell enabled rapid progress in biofuel cell assembly and miniaturization efforts.[7-11]

Despite recent advances towards higher power outputs[12-15] and implantability of miniaturized biofuel cell assemblies,[16-18] their lack of long-term stability remains an issue. For applications in consumer devices or in surgical implants, system lifetime must be extended to the order of years.[5,18] Permanent and effective electrical wiring of the protein's active centers to bulk electrodes is a crucial factor for the assembly of durable fuel cells with successful electrical communication with the current collectors. Furthermore, an increase in efficiency of fuel cell outputs might be achieved through deeper oxidation of biofuels and multi-substrate designs of electrodes, provided that applied enzymatic reactions do not compete with each other.[19,20] Also the development of nano-engineered devices for cascade reactions of immobilized enzymes in terms of direct or mediated electron transfer are likely to improve the usability of enzymatically catalyzed redox reactions for electrical power generation.[21,22] The core subjects covered within this thesis are introduced in the following subchapters.

1.1 Principles of Heterogeneous Electron Transfer for Bioelectrocatalysis

Pivotal in the construction of enzymatic electrochemical sensors and biofuel cells is achieving electrical contact between the redox proteins and electrode supports. Most redox enzymes do not support direct electrical communication between their redox active cofactors and current collectors, as the biocatalytic centers are surrounded by a protein shell that imposes a steric hinderance. This typically insulates the enzymes electrically, resulting in redox centers of proteins that cannot be regenerated by the potentials applied to the electrodes.[23] This effect is explained by the existance of tunneling barriers in the electron transfer theory by Marcus et al.,

Equation 1.1.[24] The theory proposes that the electron transfer rate k_{ET} between a donor-acceptor pair is exponentially dependent on the distance d separating them, with d_0 being the Van der Waals distance and ΔG° and λ_0 as the free energy change and the reorganization energy that are accompanying the electron transfer process. The tunneling barrier parameter β depends on the chemistry and structure of the junction.

$$k_{ET} \propto e^{-\beta(d-d_0)} e^{\frac{-(\Delta G^\circ+\lambda_0)^2}{4RT\lambda_0}} \qquad (1.1)$$

The enzyme's redox center and the electrode surface can be regarded as a donor-acceptor pair (or vice versa), whereas the protein shell surrounding the active site of the enzyme represents the spatial separator and kinetic modulator of electron transfer.[25] This electron transfer barrier must be overcome to yield electrical communication. Two main approaches are established for bioelectrochemical systems, direct and mediated electron transfer. In direct bioelectrocatalysis, suitable enzymes need to be aligned to yield sufficient proximity between the redox centers and electrode surface for electron transfer.[26-28] The redox centers are regenerated directly at the electrode upon substrate conversion. Only few enzymes are known to be capable to perform direct electron transfer (DET), such as enzymes with redox-active metallo-centers in their active site, e.g. heme, iron-sulphur cluster, and copper like peroxidases, or also fructose dehydrogenase (FDH) and several other oxidoreductases.[29-33]
Copper-containing enzymes such as laccase[27,34] (LAC) and bilirubin oxidase[35-37] (BOD) were targets for investigating DET. For these enzymes DET bioelectrocatalysis was especially effective on nano-structured carbonaceous electrode surfaces.[38-42]

In mediated electron transfer (MET), redox-active relay units are introduced to bridge the electron transfer insulating gaps. The enzyme catalyses the oxidation or reduction of the primary substrate in form of a fuel or oxidant while subsequently the enzyme transforms the mediator molecule. The regeneration of the mediator occurs at the electrode surface.[3] To enable minimal thermodynamic voltage losses for biofuel cells, the redox potential of a mediator should be close to the redox potential of the enzyme. Various methods to incorporate mediators exist, ranging from diffusional mediation within the electrolyte,[43,44] tethering of relay molecules by covalently binding them to matrices or enzymes,[45-47] or by immobilizing the enzymes in redox polymer matrices.[48-50] We previously introduced a promising design for enzyme wiring by encapsulating mediators in mesoporous carbon nanoparticles (mCNPs).[51] This approach was also shown to be suitable for bi-enzymatic electrode modification.[52]

1.2 Enzymatic Cascades

The high specificity of enzyme-substrate interactions supports biocatalytic transformations within highly heterogeneous fluids, which is an important advantage for biofuel cell application. Because of this high specificity, single enzyme electrode based fuel cells are likely to be restricted to one exclusive fuel and oxidizer. Since most studies on enzymatic biofuel cells (EBFCs) employ single enzyme electrodes, they generate current through one enzymatically catalyzed transformation step per electrode. In these cells, any remaining chemically stored energy is wasted, as are other potentially exploitable substrates in the feed solution. In order to harness more energy from these substances and thus to broaden the functionality of EBFCs, electrodes can be modified with several enzymes working in parallel or

cascading processes. Anodic multi-enzymatic assemblies have been applied for the deep oxidation of various substrates including alkanes,[53] ethanol,[54,55] glucose,[56-58] glycerol[59,60] maltose,[61] methanol,[62-64] and starch.[65] Also sucrose, commonly known as table sugar, is an attractive molecule for alternative energy supply. The hydrolysis of sucrose to glucose and fructose by the enzyme invertase (INV) was shown in a cascaded biofuel cell by Hickey et al..[66]

It should be noted that most of the multi-enzymatic biofuel cells reported so far deliver rather low power outputs, which can be attributed to bottlenecks in the kinetics of certain cascade steps, inefficient tuning of the anodic redox potential, or an unsatisfactory electrical communication between the enzymatic cofactor sites and the current collectors.[19] To guarantee high-yield power output in cascaded enzymatic fuel cells, the cascadic pathways must be efficient and avoid side reactions and crosstalk between the anode and the cathode. Sufficiently high turnover rates of the concerned enzymes involved will be a crucial factor in multi-enzymatic electrode assemblies.

1.3 Cathodic Oxygen Reduction

In contrast to the large selection of possible fuels operating at the anodes, in almost all reported cases oxygen is used as the primary oxidizer in biofuel cells. The modification of electrodes with blue multi-copper oxidases, i.e. LAC or BOD, has long been known to enable the bioelectrocatalytic reduction of oxygen to water at sufficiently high potentials.[67-69] The applicability of such enzymatically modified cathodes for biofuel cells that operate in aerobic environments and their performance in biological fluids have thoroughly been demonstrated.[70-72] Still, it remains a scientific challenge to this

date to overcome the kinetic restrictions associated with the low turnover rates of these specific enzymes.[73,74] Considering alternatives for biocathode functionalization, only few examples were reported that do not directly use oxygen as an oxidizer.[75-80] The operation of EBFCs is therefore presently largely limited to aerated environments. The design of novel electrode configurations, and especially effective bioelectrocatalytic cathodes, is a challenge that needs to be resolved in order to increase the overall performance and applicability of biofuel cells.

1.4 Operational Lifetime of Enzymatic Biofuel Cells

As mentioned above, the long-term decrease in biocatalytic performance originating from the inevitable time-dependent degradation of the biological components poses a significant challenge for the successful implementation of biofuel cells. A direct observable consequence is a gradual deterioration in discharge performance of EBFCs over time, which limits both their operational lifetimes and shelf lives. This restricts their applicability for commercial devices. The deterioration of catalytic activity and the resulting loss of cell power can be attributed to an accumulation of time-dependent effects. These include biofouling of the active surfaces, denaturation of the tertiary structures of the biocatalysts that effect their activity, and possible release of bound enzymatic biocatalysts into the electrolyte.[81,82] To a certain extent, the application of polymers or gels is beneficial to protect the integrated protein architectures and minimize degradation effects. However, these matrices introduce additional diffusion barriers for substrate and product molecules of the enzymatic transformations, resulting in a slowdown of turnover rates and subsequent

performance loss. Additionally, the use of molecular mediator molecules can have negative implications on the operation and lifetime of the cells in terms of leakage from the assemblies or destructive effects on the protein backbone upon covalent binding.[83,84] As these factors affecting the discharge durations may be reduced yet not averted, alternative solutions are needed.

In order to overcome the limitations of operational lifetimes for enzymatically modified electrodes, there is urgent need for concepts that allow in-situ replacement of active electrode substances to guarantee seamless operation independent of the enzymatic stabilities. The use of magnetizable components appears attractive due to the possibility of non-invasive control by an external magnetic field.[85] The functionalization of magnetic particles provides attractive opportunities, i.e. to translocate enzymatic biocatalysts within a biofuel cell towards or away from a current collector. The use of magnetic components has been of an interest to the field of bioelectrochemistry, with several reported studies investigating the control of magnetic fields over the electrochemical acitivity of enzymatically functionalized electrodes.[86-89] The combination of magneto-assisted biocatalysis and the emerging field of DET bioelectronics looks promising with regard to stability, as avoiding mediator molecules circumvents potential long-term leakage effects and destructive enzyme-relay modifications.

1.5 Objectives of the Thesis

The focus of this doctoral thesis is to design and investigate embedded enzymatic cascades on nanoengineered electrodes, aiming to broaden the range of alternative fuel and oxidizer resources in biofuel cells and to increase the efficiency of substrate oxidation. Building on that, we attempt to develop concepts to increase the operational lifetimes of these cells in view of future electronic applications.

Chapter 2 provides a brief introduction to cyclic voltammetry, the primary method used in this work for characterizing the bioelectrocatalytic functions, electrical contacting, charge transfer mediation and electrode stability.

Chapter 3 introduces a multi-substrate operated anode based on an enzymatic cascade allowing the deep oxidation of sucrose. Carbonaceous matrices and suitable redox mediators are discussed and tested. Furthermore, we highlight the capability of multi-enzymatic electrode assemblies to oxidize a variety of fuels.

In an effort to diversify the operating conditions of enzymatic biofuel cells, in Chapter 4 we demonstrate a cathode that functions under both aerobic and anaerobic conditions. The traditional oxygen dependent bioelectrocatalysis of BOD is complemented by an alternative route in which hydrogen peroxide serves as an internal source supplying the oxygen oxidizer via an additional enzymatic step.

In Chapter 5 we pursue the goal to reversibly switch ON and OFF DET-bioelectrocatalysis by external magnetic triggers. As a part of this effort, we translocate enzymatically modified magnetic nanoparticles by changing magnetic field gradients. A simultaneous control over the channeling of magnetic nanoparticles of either single or multi-enzyme architectures and supporting anodic/cathodic DET

pathways allow the switchable generation of power outputs in the respective biofuel cell assemblies.

In Chapter 6, we demonstrate an effort to extend the operational lifetimes of enzymatic biofuel cells. To this end, we employ enzyme-modified magnetic components to reenergize biofuel cells after exhaustion of their biocatalysts through a deep stage discharge.

2 Fundamentals of Electrochemical Analysis

This chapter provides a brief introduction to the electroanalytical method of cyclic voltammetry and the kinetic study of electron transfer reactions. It is intended to facilitate interpretation of the results presented in the following chapters and, to this end, focuses on models well established in literature.

2.1 Voltammetric Analysis

In electrochemistry, cyclic voltammetry is a standard analysis tool to characterize mechanisms of heterogeneous and homogeneous electron transfer reactions. It provides insights on the thermodynamics of redox processes and information on the kinetics of electron transfer and associated chemical reactions.[90] In order to record a cyclic voltammogram (CV), a variable electrode potential is applied and the system's current response is detected. The results are plotted in a current-voltage diagram. To perform a cyclic-voltammetry measurement, a working electrode is immersed into the electrolyte. This electrode serves as current collector and detects heterogeneous electron transfer and different other phenomena related to the electrochemical interface, including the observation of charging currents and mass transport of electro-active species. A defined shape of the electrode and therefore a controlled surface area is required for reproducible cyclic voltammetry results. As the measurement of an absolute potential of a single electrode is not possible, the potential of the working electrode, WE,

is ideally measured against a non-polarized reference electrode, RE. In the common three-electrode setup, as illustrated in Scheme 2.1, an additional counter electrode, CE, balances the charge passing on the working electrode, WE, to ensure the stability of the reference electrode.[91] The CE often has a much larger surface area than the working electrode to avoid limiting the reaction process.

To record a CV, a potential E_1 is applied to the working electrode and linearly increased or decreased, Figure 2.1 (A). The potential is varied at a constant speed $v_{scan} = \frac{dE}{dt}$, referred to as scan rate. If an electrochemical species B in the electrolyte gets to the vicinity of the electrode and the redox potential of B lies within the applied potential range, it has a chance to undergo an electrochemical reaction with a current response similar to the one depicted in Figure 2.1 (B). Here we consider a common case, where B can diffuse freely. The characteristic shape, depicted for a non-stirred electrolyte, results from the different equilibrium states for each potential $E(t)$ of the redox reaction of the detected molecules, Equation 2.1.

$$B_{ox} + z_e e^- \leftrightarrow B_{red} \qquad (2.1)$$

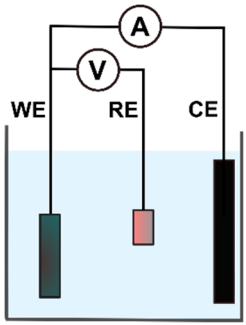

Scheme 2.1 Illustration of an electrochemical three-electrode setup

The number of electrons z_e per reduced or oxidized molecule are summed up to constitute the measured current. The potential dependence of the equilibrium concentrations of oxidized B_{ox} and reduces molecules B_{red} is known from Nernst equation, Equation (2.2), under consideration of standard electrode potential $E°$ of the species, the absolute Temperature T, Faraday constant F, and the universal gas constant R.

$$E = E° + \frac{RT}{z_e F} \ln \frac{[B_{ox}]}{[B_{red}]} \qquad (2.2)$$

At electrode potentials below the component's redox potential, the molecules in the vicinity of the electrode are increasingly reduced, while at more positive potentials the molecules of this species are rather oxidized. Within the linear sweep of potential from E_1 to E_2, given that in this example E_2 is more positive that E_1, the redox active species in the vicinity of the electrode is driven to pass different equilibria dictated by $E(t)$ from all B_{red} to all B_{ox} molecules.[92] Accordingly, the equilibrium in Equation 2.1 is shifted to the left side. The curve shapes are affected by the mass transport of the molecules to and away from the electrode surface. An anodic current peak i_p^a at the potential E_p^a can be observed during the potential sweep. It indicates that mass transport limitations on the surface effect the current. At this point the kinetic control is shifted from the maximal rate of electron transfer to the rate of mass transport as the concentration of unreacted molecules B_{red} at the electrode surface is depleted.[92] The following decrease of current reflects the diffusion controlled reaction, which in this simplified example follows Fick's second law of diffusion for the oxidized species with its immanent diffusion coefficient D, Equation 2.3.

$$\frac{\partial[B_{red}]}{\partial t} = D_{B_{red}}\left(\frac{\partial^2[B_{red}]}{\partial x^2}\right) \qquad (2.3)$$

Equation 2.3 predicts the time dependence of the local concentration change of B_{red} due to diffusion gradients, here given as a one-dimensional approach, and explains the depletion of B_{red} at the electrode surface ($x = 0$) under constant oxidation of B_{red} with the rate $\frac{\partial[B_{red}]}{\partial t}$. The CV is completed by a back sweep of potential from E_2 returning

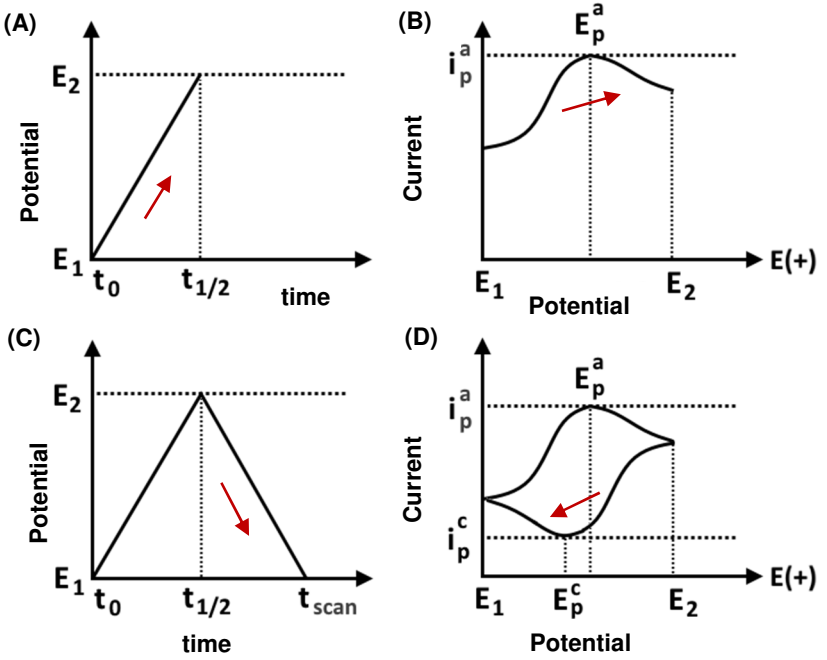

Figure 2.1 Diagrams of an exemplified cyclic voltammetry measurement for a reversible redox couple: (A) Linear change of the applied potential as a function of time in a single sweep (forward scan), (B) Current response of the system to the single sweep, (C) complete potential cycle including the backwards scan, and (D) the completed cyclic voltammogram current response. The red arrows indicate the direction of recording.

with the same scan rate to the initial potential E_1. This triangle-shaped potential, see Figure 2.1 (C), is referred to as one cycle. If the redox active species undergoes a fully reversible redox reaction as in Equation 2.1, without any side reactions, the backwards scan results in a cyclic-voltammetry response of the system as exemplified in Figure **2.1** D. When the applied potential is reversed, it reaches the potential that re-reduces the product formed in the first oxidation reaction, and produces a current of reverse polarity from the forward scan. The reduction peak in this case has a similar shape to the oxidation peak and the ratio of the anodic and cathodic peak current is ideally equal to one, Equation 2.4.

$$\left|\frac{i_{a,p}}{i_{c,p}}\right| = 1 \tag{2.4}$$

For reversible heterogeneous electron transfer reactions the peak potential is independent from the scan rate. When the heterogeneous electron transfer at the electrode surface is fast and the current response is controlled by the planar diffusion of the molecules to the current collector, the peak current behaves proportionally to the square root of the scan rate, Equation 2.5.

$$i_{a,p} \ and \ i_{c,p} \propto \sqrt{v_{scan}} \tag{2.5}$$

In this case, also the peak-to-peak separation has a defined distance, Equation 2.6. The redox potential can be read out as the mean anodic and cathodic peak, Equation 2.7.

$$\Delta E_p = E_p^a - E_p^c = \frac{59}{z_e} mV \ (at\ 25℃) \tag{2.6}$$

$$E° = \frac{E_p^a + E_p^c}{2} \qquad (2.7)$$

This behavior does not apply if the rate constants of reduction and oxidation reaction differ. In such quasi-reversible reactions, the applied scan rate defines the shape of the voltammogram. The current responses may also vary in cases such as chemically modified or adsorbed species on the electrode surface, the introduction of forced convection into the electrolyte, i.e. by mechanical stirring or gas purging, or migration effects of charged species exposed to the electrical field within the cell. Most importantly, the current response characteristically changes if reactants are subject to other chemical reactions.

2.2 Cyclic Voltammograms Involving Homogeneous Electron Transfer Reactions

Oxidized or reduced species of the examined redox active species may undergo further chemical reactions with other components present in the electrolyte. A CV does only report the reactions involving the electrode surface, however the absence and change of the current peaks and redox potentials indirectly points out other reactions taking place. We differentiate between heterogeneous and homogeneous electron transfer reactions. In the following we use a common abbreviation for reactions in an electrochemical cell first suggested by Testa and Reinmuth.[93] Electrochemical reactions are marked as **e**-type, meaning that a heterogeneous electron transfer to the current collector occurs. A chemical reaction is labeled as **c**-type when it is takes place between molecules in the electrolyte, namely homogeneous electron transfers. Equation 2.1 therefore poses a **e**-type reaction mecha-

nism, when the involved electron transfer occurs to or from the electrode. If the oxidized species should undergo a further **c**-type reaction to form an unreactive product *U*, the whole reaction is labeled as **ec**-mechanism, Equations 2.8.

$$\begin{aligned} \boldsymbol{e}\text{: } & B_{ox} + z_e e^- \leftrightarrow B_{red} \\ \boldsymbol{c}\text{: } & B_{ox} \xrightarrow{k_{ec}} U \end{aligned} \qquad (2.8)$$

This way, the time dependent concentration change of B_{ox} is not only diffusion controlled but influenced by the kinetics of the **c**-reaction with rate constant k_{ec}, Equation 2.9, assuming a first order reaction.

$$\frac{\partial[B_{ox}]}{\partial t} = D_{B_{ox}}\left(\frac{\partial^2[B_{ox}]}{\partial x^2}\right) - k_{ec}[B_{ox}] \qquad (2.9)$$

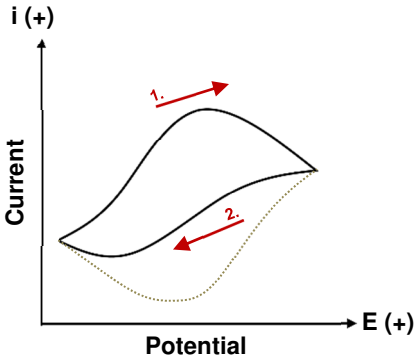

Figure 2.2 Exemplaric CV of an ec-type reaction mechanism with a high rate constant of the chemical reaction of the oxidized species. The arrows indicate the sweep direction. The dashed line indicates the backwards scan for the reversible case (e-mechanism).

The resulting CV provides insight into the rate constant of the chemical reaction. Exemplarily, we show here a CV of an **ec**-type mechanism with a high k_{ec}, Figure 2.2. The electroactive species is oxidized like above in the forward scan, yet the reduction peak of the reversing reaction in the back scan is hardly visible as the subject of reduction B_{ox} is rapidly converted to U. The height of the backwards scan peak and a variation of the applied scan rate can give insight into the magnitude of k_{ec}.

More complex reactions can be analyzed via cyclic voltammetry, for instance if the intermediate product U again forms an electroactive molecule that interacts with the current collector, resulting in an **ece**-type reaction mechanism. These types of CVs can contain several peaks that largely depend on the redox potentials of both electroactive species, the applied scan rate, and the rate constant of the chemical reaction.

For the bioelectrocatalytic experiments that are subject of this thesis, an altered version of the **ec**-mechanism best describes the reactions taking place. The so-called **ec'** reaction mechanism is used when the homogeneous electron transfer step involves a catalytic process, indicated by the **c'** label.

$$\begin{aligned} \boldsymbol{e}&: \; B_{ox} + z_e e^- \leftrightarrow B_{red} \\ \boldsymbol{c'}&: \; B_{ox} + S \xrightarrow{k_{ec'}} B_{red} + P \end{aligned} \tag{2.10}$$

In this scenario, the original electroactive substance B_{red} is regenerated by a substrate S to its originial state, Equations 2.10, opposed to the regeneration in the backwards scan at the electrode. In the catalytic reaction, S is simultaneously reduced to a product P.

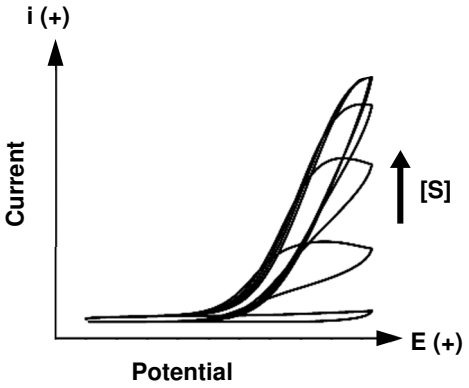

Figure 2.3 CVs showing the current responses of an ec' reaction mechanism based system upon varied substrate concentrations. This example shows the catalyzed oxidation of glucose via GOX in non-saturated regimes.

In bioelectrocatalysis, *B* may be regarded as the active center of the enzyme catalyzing the transformation of *S,* the molecule communicating the biocatalytic step to the electrode surface. Here, the illustrative process would describe a redox protein that biocatalyzes an anodic process, as *S* is oxidized and electrons are transferred from the current collector. Figure 2.3 shows generic CVs for this type of reaction mechanism for increasing concentrations of *S*. The lowest current response exemplifies the fully reversible **e**-type reaction of B_{ox} for the case that no substrate is added to the system. Upon addition of *S*, the reduction peak in the back sweep is absent, similar to the **ec**-type response. However, the oxidation peak is substantially increased, provided the scan rate is small enough to allow a sufficient measurement time for the catalytic process with the rate constant $k_{ec'}$ to take place. The higher catalytic currents occur due to the regeneration process of B_{red}, which therefore can react

multiple times at the electrode within one sweep. As the concentration [*S*] is increased, the regeneration process is enhanced and the current response rises accordingly. Furthermore, the oxidation of B_{red} is thermodynamically enhanced, as the electrochemical equilibrium state according to Nernst equation at each point of the sweep is the driving force to produce more B_{ox} molecules. As those are chemically oxidized by th **c'**-reaction, the system is further away from balance and the electrode conversion further shifted towards oxidizing more B_{red}. This process may have an impact on the slope of the current.

2.3 Kinetics of Enzymatic Substrate Conversion

Biological catalysts require a few explanations regarding their kinetic impact on cyclic voltammetry measurements. Apart from the influence of the diffusion limitations of the substrate, the current response of the system is controlled by the kinetics of the enzymatic catalysis.[91] Electron transfer rate constants with involved enzymatic catalysis, so called turnover numbers k_{et}, are typically low (below 100 e^{-} s^{-1} for certain enzymes),[94] and are influenced by the quality of electrical contacting and the rate of the substrate conversion by the enzyme k_{cat}. Therefore, in order to detect enzymatically catalyzed reactions via cyclic voltammetry, low scan rates, i.e. 1 to 20 mV s^{-1}, are applied.[95,96] Additionally, it needs to be noted that in contrast to the pattern shown in Figure 2.3, bioelectrocatalytic peak currents will not infinitely rise upon increase of [*S*]. The peak current responses saturate as depicted in the inset of Figure 2.4, upon increase of [S]. The saturation current corresponds to the maxmimal conversion speed $v_{max} = k_{cat}\,[E]$ of the enzyme-substrate combination, [*E*] being

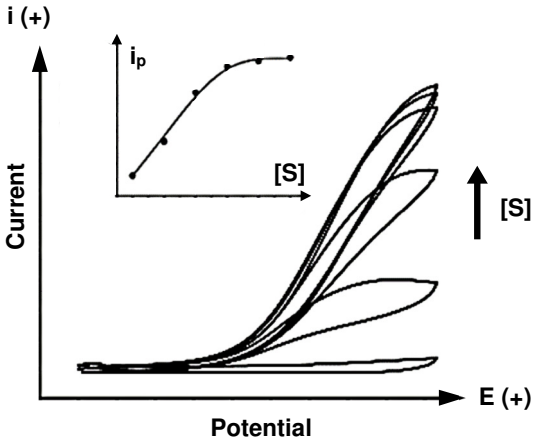

Figure 2.4 Cyclic voltammograms showing the current responses for successful bioelectrocatalysis with increasing substrate concentrations [*S*] for the redox enzyme. In this example, fructose dehydrogenase catalyzes the oxidation of fructose.

the concentration of catalytically active enzyme. The conversion speed v_{cat} is likely to be the rate limiting step of the electron transfer mechanism, hence the change of the peak current upon increase of [*S*] is governed by the conversion speed when the system is not diffusion controlled.[95] The asymptotic behaviour of the enzymatic reaction speed typically is described by the Michaelis-Menten model,[96] Equation 2.11, although it should be noted that the model is based on certain assumptions that may not always apply.[94] The model predicts that the speed of the catalyzed reaction v_{cat} depends on the initial concentration of the substrate [*S*] and the reaction specific Michaelis constant K_M.[97]

$$v_{cat} = k_{cat} \frac{[E][S]}{[S]+K_M} \qquad (2.11)$$

The Michaelis constant K_M is defined as the substrate concentration at which the reaction rate is at half-maximum and therefore is a measure for the substrate's affinity for the enzyme. K_M varies for different possible substrates for the same enzyme.[98] The behaviour of v_{cat} upon increase of [S] and electrical communication effects determine the saturation curve for the heterogeneous electron transfer reaction in non-diffusion controlled regimes.

3 Multi-Substrate Driven Bioelectrocatalysis

To exploit chemical energy stored in fuels more efficiently we foresee significant benefits from electrodes modified by multiple enzymes working in parallel or showing cascading functions. Such electrodes not only would broaden the range of fuels suitable for enzymatic biofuel cells but also enhance current collection from the fuel available. In this chapter, we show a bioanode that is capable of operating in fructose, glucose, sucrose, or a combination of these. In an effort to achieve deeper oxidation of fuels, we propose extracting four electrons from a single molecule of sucrose through the use of a multi-enzymatic cascade. The cascade steps and the electron transfer pathways including the mediation redox processes and suitable conductive surfaces are discussed.*

3.1 Carbonaceous Conductive Matrices in Bioelectrochemical Applications

Carbon-based nanomaterials attract interest as functional materials for electrical contacting of redox systems with electrodes.[99-101] Apart from being cheaper than conventional catalyst supports and their high conductivity, the carbon surface is resistant to both acidic and basic media and stable over a large range of temperature. Also advantageous is the possible modification of the chemical properties of the

* This chapter has been published in part in K. Herkendell, R. Tel-Vered, and A. Stemmer, "Switchable aerobic/anaerobic multi-substrate biofuel cell operating on anodic and cathodic enzymatic cascade assemblies", *Nanoscale*, 2017, **9**, 14118-14126.[21]

surface to control and adjust polarity and hydrophobicity of carbonaceous supports. Recent research in this field mainly focused on carbon nanotubes, nanofibers, and graphene.[102-105] Carbon nanoparticles combine the described properties and large surface areas that provide niche architectures well suited to fuel cells, sensors, and bioelectronics. Certain carbonaceous nano-architectures, like single- or multi-walled carbon nanotubes, have dimensions that are unique for direct electronic interactions with redox proteins, as similar size scales can enable the formation of synergistic bio-nano hybrids.[106] Additionally, the mentioned possibilities to chemically functionalize the carbon surface (e.g., amine-, carboxyl-, hydroxyl-groups), can provide additional sites for specific redox protein attachment.[16,107] Apart from that, the adsorption of different redox enzymes, such as LAC or BOD, on carbonaceous nanostructures may lead to partial unfolding of the proteins, thus, allowing direct electrical communication of the enzymatic redox centers with the conductive carbon surface and the electrical wiring of the resulting hybrids with electrode supports.[108]

Recently, mesoporous carbonaceous materials gained increasing attention as matrices for enzyme-modified electrodes due to the excellent electrical conductivity, high specific surface areas and a narrow mesopore-size distribution of the former.[109,110] Based on these favorable characteristics, we previously introduced mesoporous carbon nanoparticle, mCNP, matrices as unique multi-functional supports for EBFCs.[51] These systems are based on the encapsulation of relay units inside the nano-sized pores of the mCNP matrix by capping the pores with the redox enzymes desired for bioelectrocatalytic transformations. Through the efficient electron transfer between the active center of the enzymes that are capping the pores and the trapped re-

lay units, fully integrated stable systems can be obtained, demonstrating effective bioelectrocatalysis. This methodology of enzymatically functionalized mCNPs is used as the underlying wiring mechanism in the experiments shown within this and the following chapter.

3.2 Mediating Units

Due to the mechanisms described in Chapter 1.1, most redox enzymes need to be assisted by specific relay molecules in order to be able to perform bioelectrocatalysis. For example, GOX typically requires an electron relay to wire its FAD (flavin adenine dinucleotide) cofactors to the conductive matrix because of the electrically insulating nature of the protein surrounding the redox active site, particularly when immobilized in a random orientation. Certain enzymes used within this work, namely FDH and BOD, have demonstrated evidence for direct electron transfer on different carbonaceous substrates.[111,112] Nevertheless, the use of electron relays was previously reported to assist the bioelectrochemical transformations of these enzymes.[69,113]
As shown in the previous chapter, the main purpose of redox mediation is to increase the rate of electron transfer between the active site of the enzyme and an electrode, omitting the need of direct electrical communication between the enzyme's active site and the electrode surface. In case of successful wiring and a suitable enzyme-mediator combination, the rates of MET can exceed that of the direct mechanism by orders of magnitude for enzymes with hardly accessible redox centers. The selection of suitable mediator molecules depends on several factors. The mediators need to be redox-active, yet highly stable in their oxidized and reduced state, and regarding the applicability in bioelectronic devices, biocompatibility and non-toxicity are

also important factors. Nevertheless, it is very important for an effective electron transfer that the redox potential of the mediator used fits the redox potential of the enzymatic cofactor used. As described in Chapter 2, the equilibrium of molecule concentrations in the oxidized and reduced state of a redox active component at the electrode surface is ruled by the applied potential at the electrode, as described in the Nernst equation, Equation 2.2. By adding intermediate electron transfer steps via applying mediators, the enzyme-mediator electron transfer is disconnected from the direct potential control at the electrode surface. Subsequently, electron flow to and from the electrode occurs through the electrolyte due to concentration gradients of reduced or oxidized mediator species. This electron transfer can occur either by a mediator self-exchange path or by mediator molecule diffusion.[3] Accordingly, the mediator dictates the redox potential of an MET enzymatic electrode. In order to minimize the loss to the cell discharge potential upon mediator incorporation, the redox potentials of the mediator molecules should be close to those of the involved enzymatic redox centers. Apart from that, the differences in redox potential between the mediator and the biocatalyst as well as the difference in redox potential between biocatalyst and fuel or oxidant, respectively, represent the driving force for electron transfer.[3] Because of energy conservation, appropriate mediators are limited to those with redox potentials of lower absolute value than that of the chosen enzyme.

GOX and FDH, the two anodic enzymes we chose for conversion of fructose and glucose, constitute the redox steps within the cascaded deep oxidation of sucrose. These two enzymes are able to work in parallel, if mediating units can be found that can be oxidized by both proteins and therefore can be activated at the same redox potential.[114]

The glycoprotein GOX is a metalloflavoenzyme of hydrodynamic radius 86 Å with a molecular weight of about 160 kDa, containing two FAD redox cofactors and two iron moieties.[115] The active FAD centers are buried about 15 Å in the insulating glycoprotein shell, which is why, as explained earlier, the direct electron transfer with electrodes is ineffective. The oxidized form of GOX (GOX(FAD)) oxidizes ß-D-glucose (referred to as glucose) to D-glucono-1,5-lactone (referred to as gluconolactone), Equation 3.2, which then hydrolyzes to gluconic acid. Hereby the FAD center works as initial electron acceptor and GOX(FAD) is reduced to GOX($FADH_2$). Subsequently, GOX($FADH_2$) is oxidized back by the natural electron acceptor, molecular oxygen (O_2), producing hydrogen peroxide, which can be detected by oxidation at an electrode, Equation 3.3.

$$Glucose + 2\,H^+ + O_2 \rightarrow gluconolactone + H_2O_2 \qquad (3.2)$$

$$H_2O_2 \rightarrow O_2 + 2\,H^+ + 2\,e^- \qquad (at\ electrode) \qquad (3.3)$$

In the mediated catalytic process, oxygen is replaced as the electron acceptor by the oxidized form of the mediator (Me^+) to regenerate GOX(FAD) Equation 3.4. The mediator in this catalytic cycle is reoxidized at the electrode, Equation 3.5.

$$Glucose + 2\,Me^+ \rightarrow gluconolactone + 2\,Me \qquad (3.4)$$

$$2\,Me \rightarrow 2\,Me^+ + 2\,e^- \qquad (at\ electrode) \qquad (3.5)$$

Fructose dehydrogenase is a heterotrimeric enzyme incorporating FAD and heme C groups.[116] It has a molecular mass of ca. 140 kDa and catalyzes the oxidation of D-fructose to produce 5-dehydro-D-fructose, Equation 3.6. It belongs to a group of oxidoreductases that act

on the CH-OH group of donors (EC 1.1.99.). As electron acceptor, certain molecules as well as nanostructured conductive surfaces have shown to be efficient, thus, FDH can be subject to direct as well as MET.[117-119] Since oxygen is not an eligible electron acceptor for FDH,[120,121] the latter poses an attractive anodic biocatalyst for aerobic biofuel cells.

$$D\text{-}fructose + [acceptor]_{ox} \rightarrow 5\text{-}dehydro\text{-}D\text{-}fructose + [acceptor]_{red} \quad (3.6)$$

In this study, we found two molecules that were able to mediate GOX as well as FDH: Ferrocenemethanol (FcM) and tetrathiafulvalene (TTF).[51,122] FcM is an organometallic compound consisting of two cyclopentadienyl anion rings bound on opposite sides of a central Fe^{2+} ion and is a commonly applied mediator in literature. TTF is a heterocyclic molecule known as a common building block in molecular electronics,[123] but was also previously highlighted as an effective mediator for both redox enzymes FDH and GOX.[122,124] Its planar structure might be favorable for adsorption on carbonaceous substrates as π-π stacking can occur. Nevertheless, the oxygen sensitivity of TTF must be examined as it is known to reduce oxygen in acidic environments.[125] FcM as well as TTF undergo a one-electron oxidation at a potential between 0.1-0.25 V vs. a saturated calomel electrode (SCE).

To select between these two candidates for anodic mediation, FcM and TTF, as well as 2,2′-azino-bis(3-ethylbenzothiazoline-6-sulfonic acid) (ABTS), were tested towards their suitability for the relay entrapment methodology described above. ABTS will be discussed in more detail in Chapter 4 as the chosen relay for the cathode. The corresponding enzymes were immobilized on top of the dried matrix on a

glassy carbon electrode (GCE), acting as caps that entrap the respective mediator molecules inside the pores. This strategy was previously proven to support an effective charge transfer that was attributed to the spatial limitations imposed on the relays inside the pores and their enhanced accessibility to the cofactors of the partially unfolded enzymatic caps.[51] The time-dependent amperometric responses associated with the different relays loaded on the mCNP electrodes and capped by the enzymes are depicted in Figure 3.1 (A). As indicated, only a minor (<10%) decrease in the initial amperometric responses was evident during the first 30 minutes of immersion, followed by a long-term stability exceeding several days. Our results indicate that the time-dependent amperometric responses of the enzymatically capped, TTF-loaded mCNP electrodes were almost unaffected by the

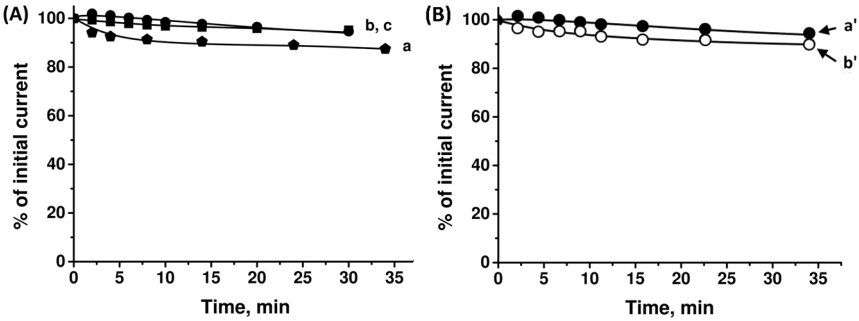

Figure 3.1 (A) Time-dependent relative current responses recorded for the mediators: (a) FcM, (b) TTF, and (c) ABTS, loaded in mCNPs-modified GC electrodes and enzymatically capped following the immersion of the electrodes for variable time-intervals. The relative values were derived by periodically performing cyclic voltammetry at 100 mV s^{-1} and indicate the peak currents obtained at E = 0.25 V, E = 0.15 V, and E = 0.50 V vs. SCE for the mediators (a)-(c) respectively, relative to the initial currents obtained before immersion of the electrodes. (B) Comparison between the time-dependent relative current responses of TTF in: (a') N_2-purged, and (b') O_2-purged buffer solution.

presence of oxygen in the electrolyte, Figure 3.1 (B). Moreover, compared to the amperometric responses by the FcM relay, under the conditions employed the TTF demonstrated a ca. 100 mV more negative redox potential, Figure 3.2. Combined with its favorable restricted leakage losses, Figure 3.1, TTF was thus selected as the primary relay molecule for our anodes.

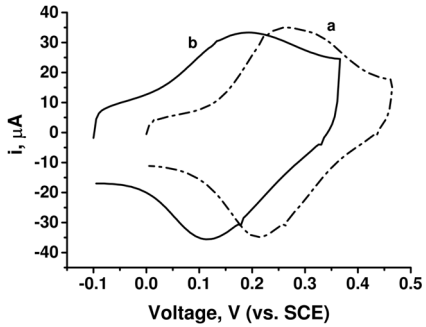

Figure 3.2 CVs corresponding mCNPs-modified glassy carbon electrodes which were loaded with: (a) FcM, and (b) TTF, and enzymatically capped. Scan rate: 100 mV s^{-1}.

3.3 Anodic Electron Transfer Pathways for the Oxidation of Multiple Sugars

The designed multi-substrate anodic half-cell in conjunction with its electron transfer pathways is depicted in Scheme 3.1. The anode hosts the enzymes INV, mutarotase (MUT), FDH, and GOX, to enable a current generation with either fructose (pathway I), glucose (pathway II), or sucrose (pathways IIIa,b). The catalytic centers of GOX and

FDH are mediated by FcM or TTF, as described above, which are entrapped inside the pores of the mCNP matrix and capped by the respective enzymes adsorbed and cross-linked on the surface. Upon their introduction to the system, paths I and II, the fructose and glucose

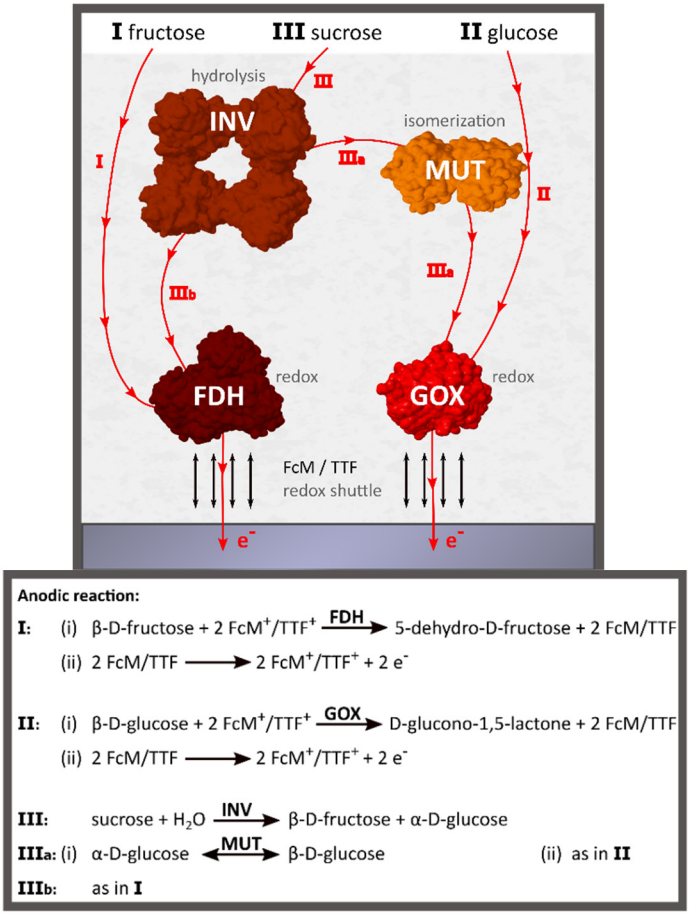

Scheme 3.1 Anodic half-cell reactions corresponding to the oxidation of: (I) fructose, (II) glucose, or (III) sucrose as substrate at the biofuel cell anode with illustration of the electron transfer pathways corresponding to the enzymatic transformations occurring at the cascaded assemblies of the anode.

fuels are directly oxidized via the mediated enzymatic catalysts FDH and GOX, respectively, to yield bioelectrocatalytic anodic currents. In contrast to the other saccharides, sucrose first undergoes an enzymatic hydrolysis by INV to yield both fructose and α-D-glucose. The fructose obtained through this reaction can, in turn, be oxidized by FDH, path IIIa, whereas the α-D-glucose requires a further isomerization to the ß-D-glucose structure before it can be electrocatalytically oxidized by GOX. This isomerization process, path IIIb, is catalyzed by the fourth enzyme incorporated into the cascade, MUT. The following subchapters show the performance of the multi-enzymatically modified electrodes when exposed to each of the possible fuel solutions.

3.3.1 Pathway I: Mediated Fructose Oxidation

When fructose is added to the anodic half-cell modified with the INV/MUT/GOX/FDH compilation, the current responses depicted in Figure 3.3 (A) can be observed. The bioelectrocatalytic currents are expected to occur solely from the conversion of fructose by FDH as described in Scheme 3.1, Equations I (i) and (ii), with the step of heterogeneous electron transfer being the recovery of two TTF mediator molecules per fructose molecule at the conductive mCNP surface, whereas the other immobilized enzymes remain inactive. The onset potential starts around 0.5 V vs. SCE and shows a linear dependency on increasing fructose concentration, saturating above ca. 60 mM as plotted in Figure 3.3 (B). As the saturation current of about 160 µA indicates the full exhaust of the FDH's capacity, the conversion speed of FDH as the rate-limiting step can be calculated according to Equation A.1 in Appendix A.5. The so-called turnover number k_{et} for FDH was estimated to be ca. 850 $e^{-} s^{-1}$, given a surface coverage of FDH on

the mCNP matrix of 20 pmole cm^{-2}, which was determined by a spectroscopic assay described in Appendix A.5. The turnover rate agrees with published values.[66,126]

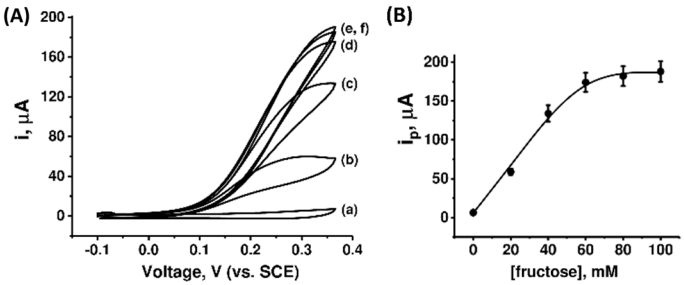

Figure 3.3 (A) CVs demonstrating bioelectrocatalytic currents obtained following the exposure of the INV/MUT/GOX/FDH-cascaded enzyme anode for 10 minutes to McIlvaine buffer solutions containing variable concentrations of fructose: (a) 0, (b) 20, (c) 40, (d) 60, (e) 80, and (f) 100 mM. (B) Calibration curve corresponding to the currents measured at E = 0.35 V for the different fructose concentrations.

3.3.2 Pathway II: Mediated Glucose Oxidation

Figure 3.4 (A) presents the catalytic currents obtained by the TTF-entrapped, INV/MUT/GOX/FDH-modified mCNP electrode upon introduction of different concentrations of glucose to the electrolyte solution. As expected, the catalytic current shows a systematic increase in amplitude for glucose added to the system, Figure 3.4 (B). As mentioned above for fructose, here the bioelectrocatalytic currents also result from 2 e^- transferred from two TTF molecules per oxidized glucose molecule, as shown in Scheme 3.1, Equation II (i) and (ii). Also

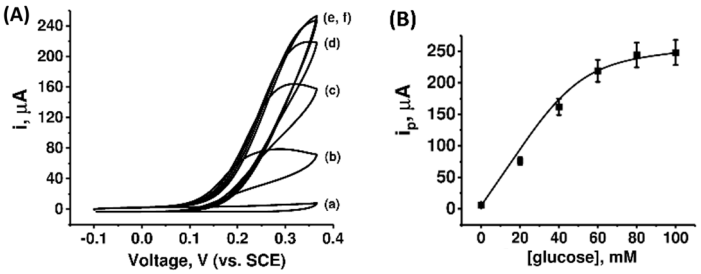

Figure 3.4 (A) CVs demonstrating bioelectrocatalytic currents obtained following the exposure of the INV/MUT/GOX/FDH-cascaded enzyme anode for 10 minutes to McIlvaine buffer solutions containing variable concentrations of glucose: (a) 0, (b) 20, (c) 40, (d) 60, (e) 80, and (f) 100 mM. (B) Calibration curve corresponding to the currents measured at E = 0.35 V for the different glucose concentrations.

here, the enzymes apart from GOX do not contribute to the biocatalysis. The system is reaching saturation above 80 mM glucose.

The comparative experiments performed in the presence of either fructose or glucose indicate that the currents obtained by the addition of glucose is higher. By spectroscopically assaying the density of the GOX on the electrodes, a similar surface coverage of FDH and GOX was obtained, 20 pmole cm^{-2}. From the saturation current density of GOX, the turnover rate for GOX was determined to be ca. 1130 e^{-} s^{-1}, in agreement with the kinetics reported in literature.[66,127] The high turnover rate for GOX suggests that this enzyme, which in order to regenerate its reduced $FADH_2$ cofactor naturally favors a path of electron transfer to its native acceptor O_2, may not be susceptible to the presence of the latter species in the system. This will be further verified and addressed in the comparative experiments presented in Figure 3.6.

3.3.3 Pathway III: Mediated Sucrose Oxidation

Gradual addition of sucrose to the buffer solution resulted in the current responses of the INV/MUT/GOX/FDH-modified anode as shown in Figure 3.5 (A). The onset potentials starting from 0.0 V suggest a successful wiring and electron transfer of the cascaded biocatalysts. The system is working under saturated conditions with a sucrose concentration above 160 mM, as can be seen from the saturation curve of currents recorded at 0.35 V for the different amounts of sucrose in Figure 3.5 (B).

The observable currents in this setup originate from the electrons harvested from sucrose via the oxidation of its hydrolysis products fructose and glucose, according to the reaction pathways shown in Scheme **3.1** III. It is conspicuous that the substrate concentrations needed to reach the saturation currents are significantly higher for sucrose, 180 mM, as compared to the direct oxidation of fructose or glucose shown in Figures 3.3 and 3.4, which saturate each below 100 mM. Whereas

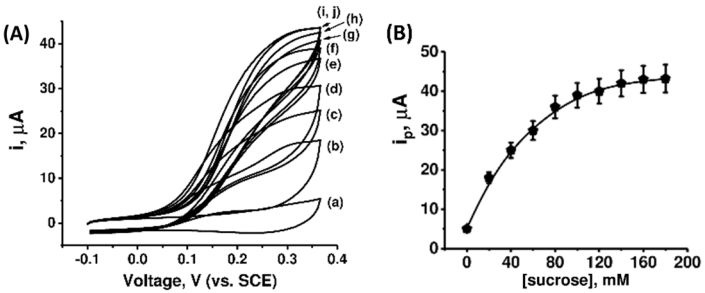

Figure 3.5 (A) CVs demonstrating bioelectrocatalytic currents obtained following the exposure of the INV/MUT/GOX/FDH-cascaded enzyme anode for 10 minutes to McIlvaine buffer solutions containing variable concentrations of sucrose: (a)-(j) 0-180 mM in 20 mM steps. (B) Calibration curve corresponding to the currents measured at E = 0.35 V for the different sucrose concentrations.

one would theoretically expect to have a full conversion of each sucrose reactant into fructose and glucose molecules, we suspect that along the diffusion paths of the product fuels towards FDH or GOX some molecules are lost to the electrolyte and cannot be recovered. Combined with the limited hydrolysis efficiency expected, this apparent phenomenon might explain the higher sucrose levels needed to saturate the electrocatalytic currents in the cascaded system.

We made further experiments with sucrose fueled electrolyte to compare the currents obtained by each of the possible combinations of enzymatic components assembled on the anode. The combinations and the resulting bioelectrocatalytic currents (at $E = 0.35$ V) are listed in Table 3.1. The findings confirm the previous results and substantiate the suggested electron pathways for the enzymatic cascade. The minor currents for the single enzyme electrode of FDH and GOX, and also all other assemblies lacking INV, can be explained by small amounts of spontaneous hydrolysis of sucrose, though smaller for GOX than for FDH in the absence of MUT, as in these cases only the autonomously mutarotated α-glucose can be oxidized.

Table 3.1 Bioelectrocatalytic current responses obtained upon challenging different anodes, based on TTF-loaded MCPs and capped by the indicated enzyme assemblies, with 180 mM sucrose solution. The indicated currents correspond to the value obtained at $E = 0.35$ V vs. SCE.

INV	x	x	x	x		x	x	x				x			
MUT	x	x		x	x	x			x	x			x		
GOX	x	x	x		x		x		x		x			x	
FDH	x		x	x	x			x		x	x				x
i, μA	43 ± 4	25 ± 4	26 ± 2	18 ± 3	9 ± 2	0 ± 0	10 ± 2	18 ± 2	5 ± 1	3 ± 1	6 ± 1	0 ± 0	0 ± 0	2 ± 1	3 ± 1

As assumed, MUT has no observable effect on fructose. Also, it can be seen that no electron transfer occurs with involment of only INV and/or MUT. For GOX, the implementation of MUT is crucial, as in its absence the natural interconversion of the α- to ß-glucose slows down the substrate supply and cuts down the bioelectrocatalytic currents of GOX by over 50%.
The results highlight the contributions of each of the cascade steps and the need to employ all four enzymes in order to amplify the overall bioelectrocatalysis. Overall, the results indicate that the multi-enzymatic assembly for the anode indeed supports the oxidation of several different fuels by providing an anodic pathway for the cascaded enzymatic reactions.

3.4 Multi-Fuel Oxidation via Enzymatic Cascades

In order to evaluate the combined effect of the different sugar fuels, we performed an additional set of measurements. Figure 3.6 presents the bioelectrocatalytic anodic current obtained upon challenging the INV/MUT/GOX/FDH-cascaded anode with a buffer solution containing all three sugar fuels fructose, glucose, and sucrose at the concentrations in which their respective saturation currents were observed. Compared to the negligible current revealed in the absence of the fuels, curve (a), an anodic current in excess of 360 μA could be detected, curve (b). Evidently, this value exceeds the saturation currents observed for the separately introduced individual fuels, suggesting that the bioelectrocatalytic process is affected by their combined contributions. Compared to the sum of individual contributions from all fuels, which would add up to ca. 460 μA, the measured value seems to recover almost 80% of the current. The observed minor losses may be attributed to the increased viscosity of the electrolyte in the presence

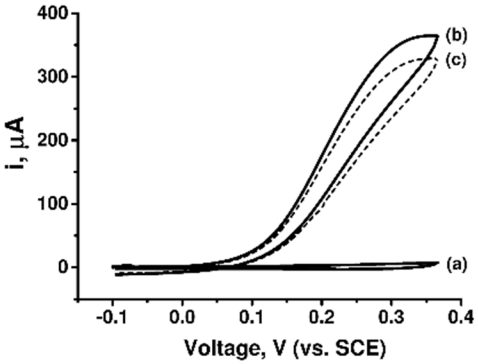

Figure 3.6 CVs showing the amperometric responses of the INV/MUT/GOX/FDH-cascaded enzyme anode: (a) in the absence of the sugar fuels, (b) in the presence of: 100 mM fructose, 100 mM glucose, and 180 mM sucrose (fuel mixture), following purging with N_2, and (c) as in (b) but following purging with O_2.

of all sugars, leading to hindered diffusion of the substrates in the system. In a further experiment, curve (c), a similar measurement was performed under O_2-saturated conditions. The results reveal a drop in the bioelectrocatalytic current from 360 μA to 330 μA at 0.35 V vs. SCE, a ca. 9% lower value as compared to the performance of the anode in the anaerobic atmosphere. This relatively modest decrease in the anodic amperometric response might be attributed to the efficient wiring of the O_2-sensitive GOX to the TTF-entrapped mCNP matrix, also in agreement with the high turnover rate that was calculated. This specific result is promising in view of our intention to further combine the multi-fuel-operated anode with a cascaded cathode system that involves O_2 consumption.

To decipher the contributions of the individual conversion processes to the overall cascadic process, we conducted several experiments showing the necessity of all enzymes to the full functioning of the anode. Figure 3.7 provides evidence for the contributions of the different enzymes to the bioelectrocatalytic anodic responses. For this purpose, in each measurement a different enzyme was omitted and the resulting electrode configurations were challenged with the fuel mixture. The occurring electrocatalytic currents were measured at 0.35 V vs. SCE. For comparison, curve (a) embodies the fully cascaded assembly with all four enzymes immobilized. When both redox enzymes FDH and GOX are immobilized on the surface, as in curves (b) and (c), the currents are significantly increased, compared to the electrodes modified with only one of the redox enzymes, curve (d) and (e). This is emphasizing the necessity of both enzymes for an efficient oxidation of the fuels. Interestingly, the contribution to the total current by electrons contributed from sucrose through INV/MUT transformations is ca. 10%, as evident from the comparison between curve (a) and the

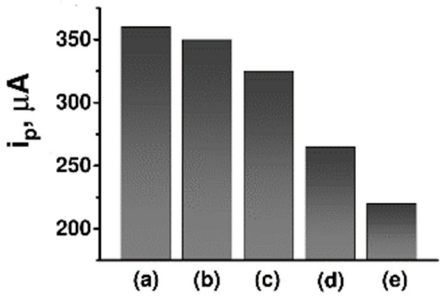

Figure 3.7 Comparison of bioelectrocatalytic currents measured at 0.35 V vs. SCE, for anode assemblies containing the following enzyme compositions: (a) INV/MUT/GOX/FDH, (b) INV/GOX/FDH, (c) MUT/GOX/FDH, (d) INV/MUT/GOX, and (e) INV/MUT/FDH in the presence of the fuel mixture.

INV/MUT/GOX/FDH-functionalized assembly, curve (c), which is lacking the INV. By eliminating the first cascade step, i.e. the sucrose hydrolysis, the resulting current expressed in bar (c) appears to represent the contribution of only glucose and fructose, as MUT is deprived of its substrate. With INV included but MUT excluded, bar (b), the total current, including the contribution by the hydrolyzed sucrose, reaches ca. 350 μA. This is to be expected considering the contribution of the INV-catalyzed hydrolysis of sucrose to its products fructose and glucose, with the latter also naturally equilibrating between its α and ß isomer forms (though at a slower rate in absence of MUT). The current responses also suggest that the transformations occurring on INV and MUT are fairly in accord with the stoichiometric breaking down of the sucrose disaccharide to its elemental fructose and glucose sugars.

Evidently, in the presence of only FDH or GOX as the redox-active enzyme components in the system, the currents reflected their separate contributions as direct catalysts for fructose or glucose oxidation, Figure 3.7, bars (d) and (e), respectively. The observation was also accompanied by a modest current via the sucrose-catalyzed generation of the sugars in the presence of INV or INV/MUT. These results are in full agreement with Figure 3.3 to Figure 3.5 demonstrating the current yields by the separate fuels on the entire cascade.

4 Cathodic Bioelectrocatalysis in Aerobic and Anaerobic Environments

A key factor of EBFC operation is the cathodic electron transfer. We aim to broaden the range of usable oxidizers and to increase the efficiency of the cathodic half-cell reaction in order to expand the operational area of EBFCs. Bioelectrocatalytic cathodes do not only limit the overall capacity and power output in most known assemblies, but in most of the cases reported they also restrict the cells to solely aerobic environments, due to the persistent use of molecular oxygen as the oxidizer of choice.[128] Here, we are pursuing the goal of making EBFCs less dependent on available oxygen sources. In this chapter, we show a bi-enzymatic cathode assembly that utilizes molecular oxygen originating either from solution phase or from an internal chemical source, as the oxidizer. The cathode employs a cascade of catalase (CAT) and BOD. The assembly involving the state-of-the-art BOD catalyzed oxygen reduction is compared to the cascaded approach, which uses hydrogen peroxide as the internal source for the oxidizer.*

4.1 Mediated Oxygen Reduction via Bilirubin Oxidase

The bioelectrocatalytic reduction of oxygen is commonly catalyzed by blue multi-copper oxidases. The modification of specific conductors

* This chapter has been published in part in K. Herkendell, R. Tel-Vered, and A. Stemmer, "Switchable aerobic/anaerobic multi-substrate biofuel cell operating on anodic and cathodic enzymatic cascade assemblies", *Nanoscale*, 2017, **9**, 14118-14126.[21]

with LAC or BOD has long been known to enable the 4 e^- bioelectrocatalytic reduction of oxygen to water at suitably high potentials.[72,129] The applicability of such biologically modified electrodes in biofuel cells operating in aerobic environments and their performance in biological fluids have been thoroughly demonstrated both in vitro and in vivo.[18,70] Nevertheless, overcoming the kinetic barriers associated with the low turnover rates of these specific enzymes remains a major scientific challenge to this date.

The oxidoreductase BOD, which will be in the focus of this work, catalyzes the oxidation of bilirubin to biliverdin with the concomitant reduction of dioxygen to water.[130] It has a molar mass of 60 kDa and contains a multi-copper catalytic center containing type 1 (T1), type 2 (T2), and type 3 (T3) coppers (in the ratio 1:1:2) similar to LAC.[69] Previously, it has been shown that the T1 site is likely to be the electron accepting center in the catalytic process while the location of oxygen transformation takes place in a T3-T2-T3 triangle shaped cluster.[131,132] The ability of BOD to reduce O_2 to water near neutral pH,[69] combined with several other biochemical properties important for biotechnological application, such as high activity, stability, and low extent of glycosylation, are attractive to biosensor and biofuel cell applications. [11,133] In its function in a bioelectrocatalytic oxygen electrode, BOD is known to be mediated by ABTS, as are other reducing enzymes with high redox potentials.[3,69] $ABTS^{2-}$ is a divalent anion that undergoes a BOD-induced oxidation to a monovalent radical, $ABTS^{\cdot-}$ at a redox potential of about 0.4-0.55 V vs. SCE. The $ABTS^{\cdot-}$ radical has a green color and is easily detected photometrically at λ_{max} = 414 nm. The BOD-catalyzed oxygen reduction in the presence of $ABTS^{2-}$ follows the reaction shown in Equation 4.1. When used to

mediate bioelectrocatalysis, the $ABTS^{\cdot-}$ radical is subsequently reduced back on the surface of the cathode, Equation 4.2.

$$O_2 + 4\,ABTS^{2-} + 4\,H^+ \rightarrow\ 2\,H_2O + 4\,ABTS^{\cdot-}\ \ (on\ BOD) \qquad (4.1)$$

$$4\,ABTS^{\cdot-} + 4\,e^- \rightarrow 4\,ABTS^{2-} \qquad (on\ electrode) \quad (4.2)$$

In literature, various strategies can be found to electrically wire BOD immobilized on carbon nanomaterials to obtain different amperometric sensors or biofuel cell elements.[134-137] As mentioned in the previous chapter, we apply a previously developed method[51] to achieve electron transfer via ABTS mediators confined to the pores of a mCNP matrix. The voltammograms depicted in Figure 4.1 indicate the formation of a BOD-catalyzed bioelectrocatalytic current when the conditions are changed from anaerobic to aerobic. Compared to the reversible redox signal of ABTS at its thermodynamic potential around 0.5 V in the absence of oxygen, curve (a), a typical BOD-catalyzed and

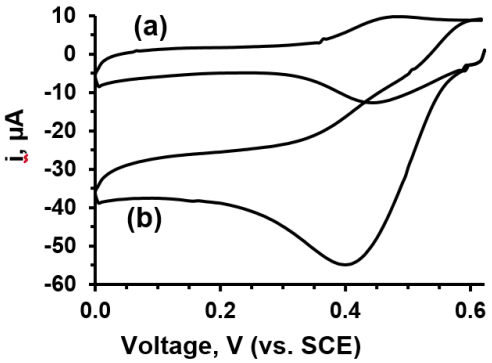

Figure 4.1 CVs demonstrating the bioelectrocatalytic currents obtained following the exposure of a BOD functionalized cathode to: (a) N_2-purged (b) O_2-purged McIlvaine buffer.

ABTS-mediated oxygen reduction bioelectrocatalytic response is observed in the presence of the substrate, curve (b). The cathodic current generated, ca. -40 μA (j = 570 μA cm^{-1}), correlates with other reports employing similar experimental conditions.[51,52]

Given the turnover rates for ABTS-mediated BOD around 100 e^{-} s^{-1}, the cathodic currents are likely to be the bottleneck of the EBFC's overall power output.[138] The limited solubility of oxygen in common electrolyte fluids and its subsequent depletion at the cathode's surface during cell operation are further problems that must be addressed during the assembly of biofuel cells.

4.2 Hydrogen Peroxide as an Alternative Oxidizer Source

Within the fuel cell elements reported in literature, only few enzymatically modified cathodes can be found that do not directly use oxygen as an oxidizer.[75-80] The need for oxygen so far limited the applicability of biofuel cells to aerobic environments as in air-breathing cathodes[36,71] or systems designed to perform in oxygen-saturated fluids as for example physiological solutions for in vivo applications.[139-142] To expand the potential of biocathodes, we sought a way to liberate the cathode from the need for directly provided oxygen by introducing into the system an alternative oxidizer source. Hydrogen peroxide constitutes an attractive option, but as a direct oxidizer it was shown to be less effective due to relatively low reduction potentials and power densities when used as cathodic substrate in biofuel cells.[75-77] In an attempt to use H_2O_2 as an alternative indirect oxidizer source, we were looking for an additional enzymatic reaction that

might trigger the release of O_2 from this substance. The enzyme catalase is known to induce the disproportionation reaction of H_2O_2, Equation 4.3.

$$2\ H_2O_2 \rightarrow 2\ H_2O + O_2 \qquad (4.3)$$

This reaction can be coupled to the four electron BOD-catalyzed reduction of oxygen to water to yield an effective CAT/BOD cascade assembly.[52] Under these conditions the CAT-induced O_2 generation already is in the immediate vicinity of the co-immobilized BOD, where it undergoes a bioelectrocatalytic reduction at approximately 0.5 V vs. SCE. In order for this strategy to be successfully implemented in compartmentless biofuel cells, the anodic assemblies must be sufficiently insensitive towards the presence of H_2O_2 in the electrolyte. To this end, we have tested the influence of this component on the bioelectrocatalytic responses of the INV/MUT/GOX/FDH-modified mCNPs

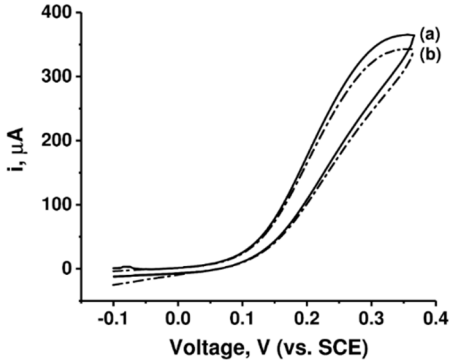

Figure 4.2 CVs demonstrating bioelectrocatalytic currents obtained following the exposure of the FDH/INV/MUT/GOX-cascaded enzyme anode for 10 minutes to McIlvaine buffer solutions containing 100 mM of glucose, 100 mM of fructose, and 180 mM of sucrose: (a) in the absence of H_2O_2, and (b) in the presence of 140 mM H_2O_2.

anode used in the multi-enzymatic approach, which was described in Chapter 3. As can be seen in Figure 4.2, a diminished effect of H_2O_2 on the anodic current generated in the presence of the sugar substrates glucose, fructose, and sucrose is observed. The minor decrease in the observed catalytic current may be attributed to the spontaneous, non-catalyzed in this case, generation of oxygen through the disproportionation reaction given in Equation 4.3. The oxygen molecules compete with the electrode on accepting the electrons produced by the catalytic reaction associated with glucose oxidation on GOX, and thus provide a minor interference to the charge transfer mechanism leading to the generation of the current.

4.3 Mediated Oxygen Reduction in Anaerobic Environments through Enzymatic Cascades

Based on our preliminary results, we have designed a cathode, which operates in both aerobic and anaerobic environments. BOD and CAT were co-immobilized on ABTS-loaded mCNPs as described in Appendix A.2. As CAT is capable of producing significant local concentrations of O_2 in the vicinity of the electrode surface, it acts as an internal source of O_2 for the BOD. This cathode is thus designed to potentially work in the absence of oxygen, namely under anaerobic conditions. On the contrary, triggering the CAT/BOD cascade with H_2O_2 when O_2 is initially present in the electrolyte solution (the aerobic state), leads to a biocatalyzed reduction of O_2 on the BOD supporting contributions from its presence both as a dissolved species, as well as from the enzymatic reaction. It should be noted that the high levels of O_2 generated through the CAT/H_2O_2 transformation provide a further advantage to the system, as the close proximity of O_2 to the cathode surface prevents significant diffusion of the species towards the anode, thus

eliminating the oxidative regeneration of the receptive reduced enzymatic cofactors, e.g. $FADH_2$, and the diminishment of the anodic bioelectrocatalytic currents. The cathode consists of ABTS-entrapped CAT/BOD-capped mCNPs deposited on a glassy carbon surface. Figure 4.3 compares the cathodic currents generated by the BOD/CAT electrode either under aerobic or anaerobic conditions, in the absence and presence of H_2O_2. The results indicate that the BOD/CAT-cascaded cathode utilizes both materials to produce the bioelectrocatalytic cathodic currents. As expected, the onset of the potentials, approx. 0.55 V vs. SCE, matches the redox potential of ABTS that is evident in the absence of both of the additives, curve (a). Evidently, the electrocatalytic cathodic current gradually increases and correlates with the increased levels of oxygen dissolved in the buffer. The aerobic cases are shown without added H_2O_2 in curves (b) with an aerated electrolyte and curve (c) with an O_2-purged solution. The introduction

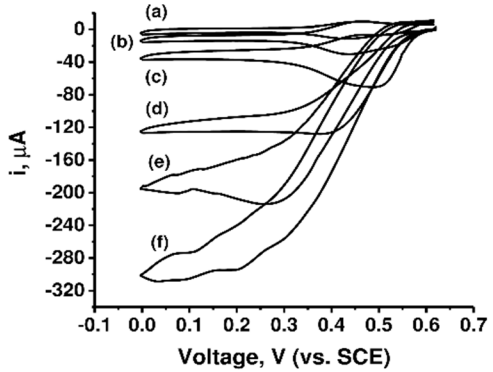

Figure 4.3 CVs demonstrating the bioelectrocatalytic currents obtained following the exposure of the BOD/CAT-cascaded enzyme cathode to: (a) N_2-purged McIlvaine buffer, without H_2O_2, (b) buffer under air, without H_2O_2, (c) O_2-purged buffer, without H_2O_2, (d) N_2-purged buffer containing 140 mM H_2O_2, (e) buffer under air, containing 140 mM H_2O_2, and (f) O_2-purged buffer, containing 140 mM H_2O_2.

of 140 mM H_2O_2 into an oxygen-free buffer allows CAT to produce a high local concentration of O_2 near the surface-immobilized BOD, exceeding the solubility levels of this species in the buffer (a few mM at ambient temperature).[143] This leads to a cathodic current increase to ca. 125 μA (at 0.0 V vs. SCE), curve (d). Interestingly, switching again at this point to the aerobic state while allowing the presence of either air or O_2 in the electrolyte in addition to H_2O_2, results in significant bioelectrocatalytic currents of ca. 195 μA and 300 μA (at 0.0 V vs. SCE), curves (e) and (f), respectively. The significant increases might be attributed to the enhanced activity of CAT in neutral to basic environments.[144] Accordingly, the four-proton mediated reduction process accompanying the O_2 transformation on BOD, elaborated in Equation 4.1, leads to a local increase of the pH at the surface of the cascade assembly. The pH shift elevates the activity of the CAT thus resulting in an autocatalytic cathodic effect.

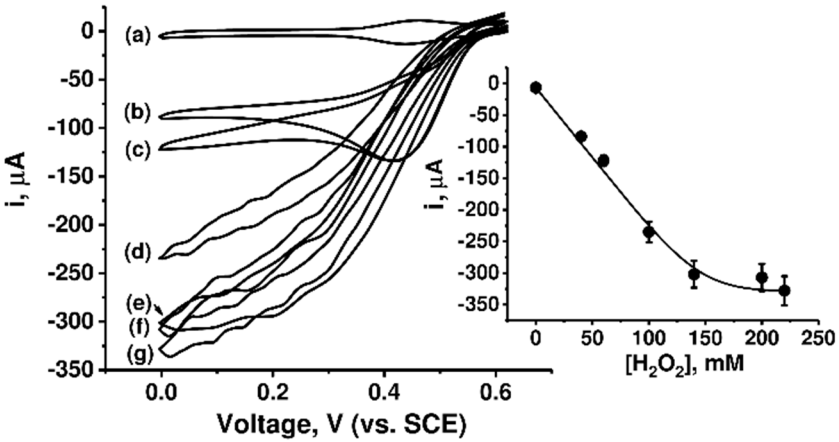

Figure 4.4 CVs showing the amperometric responses of the BOD/CAT-cascaded enzyme cathode in an O_2-prurged buffer containing: (a) 0, (b) 40, (c) 60, (d) 100, (e) 140, (f) 200, and (g) 220 mM H_2O_2. The inset corresponds to the calibration curve obtained by testing the different H_2O_2 concentrations. The reported values indicate the currents measured at E = 0.0 V vs. SCE.

The cathode's cascading behaviour was highly responsive to H_2O_2 when tested in the presence of O_2, Figure 4.4. Evidently, ca. 60 mM of H_2O_2, curve (c), were enough to generate a current similar to the one obtained upon adding 140 mM of the peroxide and testing the same electrode under anaerobic conditions, Figure 4.3, curve (d). The calibration curve presented in Figure 4.4 inset, allowed us to further estimate that under aerobic conditions the bioelectrocatalytic current of our cathode saturates at ca. 140 mM of H_2O_2. Overall, the proposed cathode operated stably and accurately tunable under anaerobic as well as aerobic conditions.

4.4 Switchable Operation of EBFCs in Aerobic and Anaerobic Environments

As demonstrated, at this stage we were able to design a cascaded biocathode that could be used in different environments according to the three modes illustrated in Scheme 4.1. The first mode is shown as electron transfer pathway IV and constitutes the "classic" way of BOD catalyzed oxygen reduction in aerobic environment, as described in Chapter 4.1. Path V depicts the anaerobic operation with H_2O_2 as single oxidizer releasing source, whereas path VI combines the mechanisms, enabling the operation of the cathode in aerobic environment (VI a) with additional H_2O_2 source (VI b).

As the cascaded anode described in Chapter 3 responded effectively to the presence of the different fuels and showed a fair insensitivity to the presence of O_2 and H_2O_2, we coupled it to this efficient enzymatic cathode. We aimed to construct a non-compartmentalized, yet multi-substrate-driven, enzymatically cascaded biofuel cell that operates in both aerobic and anaerobic states.

The designed cell is visualized in Scheme 4.2. The anode hosts the enzymes INV, MUT, GOX, and FDH, mediated by entrapped TTF molecules. The cell utilizes the three different sugar fuels fructose, glucose, and sucrose, plus O_2 as the oxidizer, and/or H_2O_2 as its internal substrate source. Figure 4.5 (A) displays the power output recorded for the cell during its discharge against variable constant external resistances. The measurements were repeated three times for

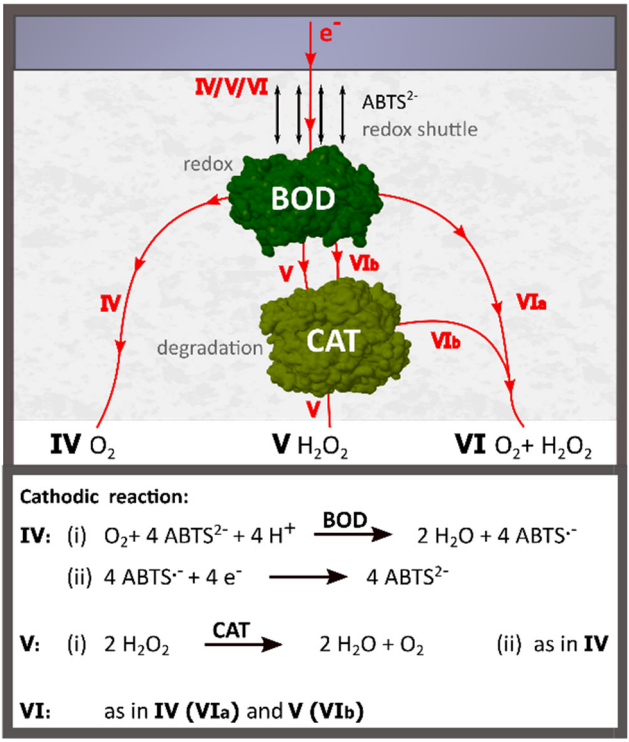

Scheme 4.1 Cathodic enzymatic cascade involving BOD and CAT mediated by ABTS. Red arrows refer to the possible electron transfer pathways and enzymatic transformations. The biocatalyzed reaction paths occurring on the cathode are shown at the bottom.

each of the aerobic and anaerobic states, curves (a) and (b), respectively, and under O_2-saturation in the absence of H_2O_2, curve (c). Evidently, under aerobic conditions, a maximal power output of ca. 240 μW cm^{-2} was obtained at a discharge current density of ca. 1.0 mA cm^{-2}. This relatively high power output was accompanied by an open circuit voltage in excess of 0.6 V, Figure 4.5 (B) curve (a), while the cell voltage during the discharge remained above an operational cut-off value of 0.2 V up to ca. 1.25 mA cm^{-2}. In comparison, the discharge of the biofuel cell under anaerobic conditions yielded a considerably lower power output of ca. 150 μW cm^{-2}, Figure 4.5 (A) curve (b), combined with a steeper voltage drop evident as the resistive load was reduced, Figure 4.5 (B) curve (b). It should be noted that the decrease in the power output during the change from the aerobic to the anaerobic states is lower compared to the values expected from the separate, stand-alone testing performed on the cathode, Figure 4.3.

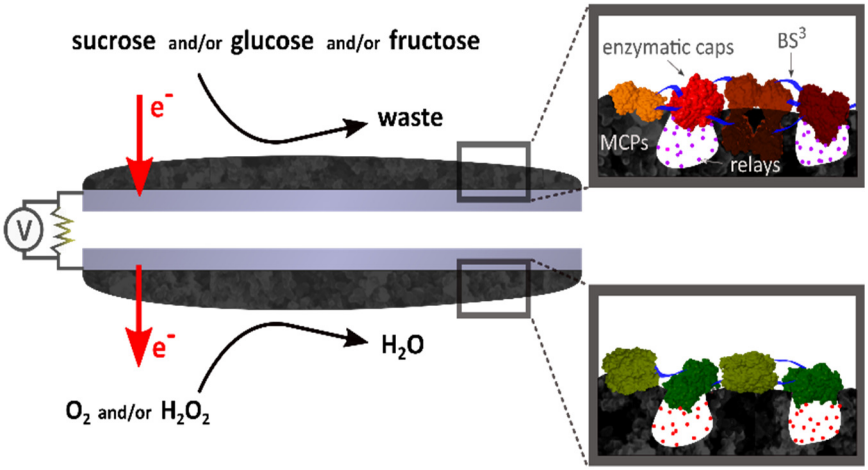

Scheme 4.2 Non-compartmentalized multi-substrate biofuel cell based on mesoporous carbon matrices containing immobilized anodic and cathodic enzymatic cascades.

One should note, however, that the reliability of such a comparison is questionable since the discharge rate of the whole cell was obtained far from the conditions applied during the sweeping of the cathode alone. Also presented in curves (c) of Figure 4.5 (A) and (B) are the biofuel cell discharge responses under O_2 saturation and in the absence of H_2O_2. A lower power output, ca. 40 μW cm^{-2}, is evident, accompanied by steep polarization losses, which are consistent with the inefficient capability of the oxidizer at its limited solubility levels to generate a significant catalytic current. This result highlights, in fact, the necessity of the BOD/CAT cascade for the enhanced functioning of the biofuel cell. As both the aerobic and anaerobic current responses of the cascaded biofuel cell were significant, we have attempted to repeatedly switch the operation modes and monitor the consistent reproducibility of the electrical power output generated. Figure 4.6

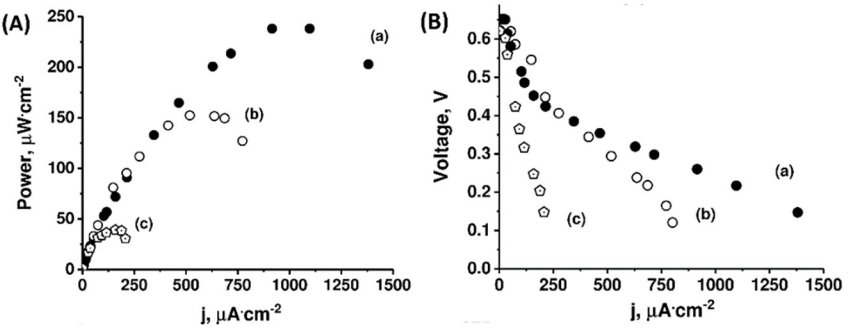

Figure 4.5 (A) Power outputs measured for the TTF-entrapped INV/MUT/GOX/FDH cascade-capped MCPs // $ABST^{2-}$-entrapped BOD/CAT cascade-capped MCPs biofuel cell upon its discharge against variable external resistances: (a) under aerobic conditions - in the presence of 140 mM H_2O_2 and saturated O_2, (b) under anaerobic conditions - in the presence of 140 mM H_2O_2 and saturated N_2, and (c) under O_2 saturation only. (B) The discharge polarization curves of the cell under the conditions described in (A). All experiments employed a mixture of 100 mM fructose, 100 mM glucose, and 180 mM sucrose fuels in McIlvaine buffer.

demonstrates the maximal power output of the cell recorded during twelve consecutive switches between aerobic and anaerobic conditions. Evidently, the cell maintained its typical discharge characteristic power (and voltage), and was seamlessly cycled between the two states for tens of times without showing significant power losses.[21]

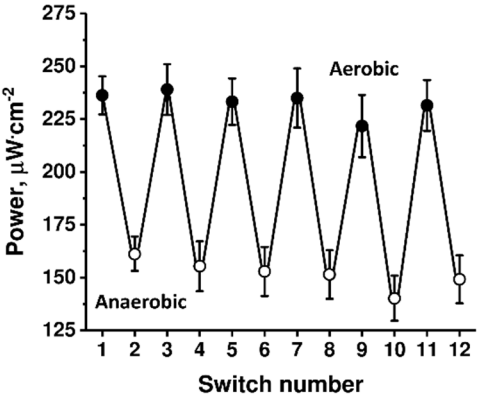

Figure 4.6 Switching the discharge of the multi-fuel, multi-oxidizer biofuel cell at its maximal power between the aerobic and the anaerobic states. The maximal power values were obtained by using external resistors allowing the cell to discharge at ca. 1000 and 600 μA cm^{-2} under the aerobic and anaerobic conditions, respectively. All experiments employed a mixture of 100 mM fructose, 100 mM glucose, and 180 mM sucrose fuels in McIlvaine buffer.

4.5 Implications for Potential Applications

The bi-enzymatic cathodic cascade assembly demonstrated an efficient operation of an EBFC under anaerobic conditions and superior power outputs in an aerobic environment when hydrogen peroxide was added as an internal oxidizer source. This makes this cathodic cascade highly interesting for compartmentless biofuel cells, since the absence of oxygen under anaerobic conditions minimizes the undesi-

red crosstalk between the electrodes in case oxygen is the natural enzymatic acceptor of anodic redox enzyme.[145] Therefore this cascade averts the often observed decrease of anodic current due to competitive reduction of O_2 to H_2O_2, e.g. by GOX in the common EBFCs. The oxygen in the system is produced locally by CAT and stays in the vicinity of the cathode, where it is immediately transformed by BOD. As this architecture can utilize either H_2O_2, or O_2, or both oxidizers together, it is also suitable for multi-oxidizer cells.

The features demonstrated, along with the relative stability, reproducible switching, and moderately high power throughput, represent a promising advance towards the construction of a new generation of versatile biofuel cells operating on mixed fuel biomass also in the absence of oxygen.

5 Magneto-Assisted Control of Bioelectrocatalysis

Being able to control EBFCs adds several advantages to their practicability: (i) on-demand operation; (ii) increase of overall lifetime as the cells can be switched on only when needed; (iii) adaptability to changing environments; (iv) biological control of electronic circuits;[146] and (v) possibility to renew active biofuel cell material in situ, extending the durability of EBFCs. Item (v) will be further discussed in Chapter 6.

In this chapter, we tried to achieve magnetically switchable heterogeneous electron transfer in order to control bioelectrocatalysis. Magnetic field actuation is an established way to influence biotechnological processes, e.g. in bioseparation.[147] Looking for ON/OFF-switching mechanisms that would allow the non-invasive interaction with the active electrode material, we found functionalized magnetic particles to be an interesting medium to work with. Here, we show a novel switching mechanism for DET biofuel cells that is applicable for single- as well as multi-enzymatic electrode assemblies.*

5.1 Magnetic Nanoparticles in Bioelectrocatalysis

Magnetic nanoparticles, MNPs, are of interest in multiple research disciplines due to their responsiveness to permanent magnets or electromagnets. Magnetic field gradients allow one to transport MNPs in

* This chapter contains parts of the publication K. Herkendell, A. Stemmer, and R. Tel-Vered, "Reenergizing enzymatic biofuel cells through magnetically assisted induction of direct electron transfer pathways", *submitted*.[148]

or collect them from suspension. Due to their small size, MNPs typically have a high surface-to-volume ratio, which makes them attractive carrier units when subjected to chemical functionalization. These features have been successfully applied in a broad range of biotechnological applications. In the biomedical field, MNPs have been shown to be carriers e.g. in immunoassays[149,150] or targeted drug delivery.[151] In the field of bioseparation, MNPs are established carrier units as they allow the separation of biocatalysts from their reaction products using external magnetic fields, which has been shown to be valuable in areas like biochemical synthesis[152,153] and environmental analysis.[154]

In terms of biosensing, some studies already demonstrated successful use of MNPs for enzymatically functionalized electrodes.[155,156] Hirsch et al. were the first to demonstrated the magnetic control of bioelectrocatalysis in 2000 by modifying magnetic particles with mediator units.[157]

The MNPs used in this study have an iron core and carbon coating with an overall average diameter of 25 nm. They show superparamagnetic behavior, i.e. they act as nano-sized ferromagnets with a high magnetic susceptibility but in bulk show the magnetization behavior of paramagnets.[158] Therefore, they can easily be magnetized by an external magnetic field and translated when magnetic field gradients are applied, but the overall magnetization becomes zero when the magnetic field is removed in contrast to regular ferromagnetic materials. The strong interaction with external magnetic fields is advantageous for our intention to switch an enzymatic biofuel cell ON and OFF by moving enzyme-modified carbon coated magnetic nanoparticles (ccMNPs).

5.2 Direct Electron Transfer Bioelectrocatalysis on Carbon Coated Iron Nanoparticles

In order to electrically contact enzyme-modified ccMNPs on an electrode surface and to analyze their electrochemical characteristics, we have built a three-electrode setup shown in Scheme 5.1. A rectangular glassy carbon slide (GC) is attached to the sidewall of a 1.0 mL cuvette as a working electrode, WE. A carbon rod as counter electrode, CE, and an SCE as reference electrode, RE, are installed in this electrochemical cell. A permanent magnet, M_1 (40x10x5 mm^3, 1.2 T, NdFeB)*, is placed behind the GC collector. Under these conditions, the ccMNPs are exposed to a magnetic field gradient upon introduction into the cell. The ccMNPs were sought to enable DET for certain redox enzymes, Chapter 3.1, due to their carbon shell. FDH and BOD were chosen as the anodic and cathodic biocatalysts, due to their reported ability to perform DET on various substrates.[30,112] The ccMNPs were interacted with buffer solutions containing FDH or BOD, as described in detail in Appendix A.3. In the case of FDH, a 1-pyrenemethylamine treatment of the ccMNPs increased the success of the immobilization. As the iron core of the nanoparticles showed a time-dependent spontaneous oxidation in commonly used buffer solutions (e.g. phosphate, acetate or HEPES buffers), we have selected MES (pH 5.5, 100 mM) as a buffer of choice throughout the study due to the enhanced stability of the nanoparticles towards rusting in this medium.[159] Following the contact adsorption process, the enzyme-modified ccMNPs were magnetically isolated and repeatedly washed with a pure buffer solution to eliminate any remains of non-adsorbed

* The magnets in the schemes are presented as horseshoe magnets for illustrative reasons, however throughout the study rectangular solid magnets were used.

protein. The resulting enzyme-modified ccMNPs were then spectroscopically assayed using colorimetric procedures described in Appendix A.5 to calculate the surface coverage values of 3 pmole FDH mg^{-1} ccMNPs and 17 pmole BOD mg^{-1} ccMNPs. The enzyme-modified ccMNPs were subsequently employed in generating DET bioelectrocatalytic currents.

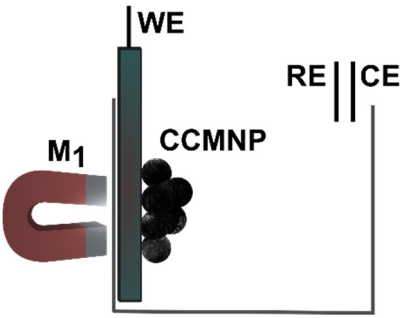

Scheme 5.1 An illustration of the electrochemical cell setup with magnetically assisted loading of the ccMNPs on the surface of the working electrode.

5.2.1 Non-Mediated Oxygen Reduction

The BOD-modified ccMNPs were magnetically loaded onto a GC electrode. Figure 5.1 presents the experiments conducted in the presence of either BOD's substrate oxygen or nitrogen. Whereas in the presence of a N_2-purged buffer no catalytic cathodic currents are observed, curve (a), upon saturating the electrolyte with O_2 a biocatalytic transformation is initiated, curve (b). Under these conditions, a cathodic current response of ca. 190 μA with an onset potential starting from approximately 0.55 V vs. SCE is evident. In this assembly a BOD turnover rate of ca. 100 $e^- s^{-1}$ is calculated. This is the first successful

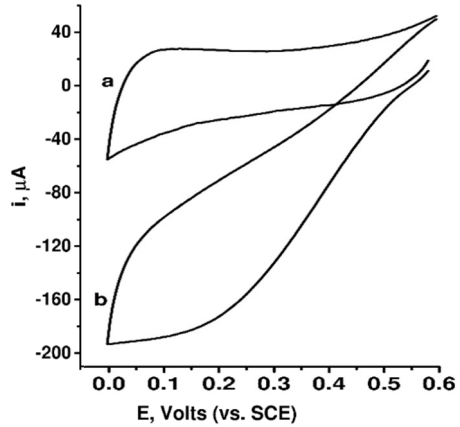

Figure 5.1 CVs corresponding to DET cathodic currents obtained by the BOD-modified ccMNPs magnetically loaded onto a GCE in (a) N_2 (b) O_2 saturated solutions.

proof of concept, showing that (i) the ccMNPs become firmly attached the current collector through M_1, (ii) the magnetized ccMNPs form electrical contact to the GC surface, (iii) BOD is electrically wired and able to perform DET when adsorbed on the ccMNP surface, and (iv) conductive paths are facilitated that enable the transfer of the electrons associated with the enzymatic transformations, leading to the observable bioelectrocatalytic currents via cyclic voltammetry.

5.2.2 Non-Mediated Fructose Oxidation

The concept of magnetically induced direct electron transfer was also tested for the FDH-catalyzed oxidation of fructose. Figure 5.2 (A) depicts the anodic current responses obtained upon directing the FDH-modified ccMNPs onto the surface of glassy carbon via the magnetic field induction of M_1. The magnet was placed behind the current collector and variable concentrations of fructose were introduced to the

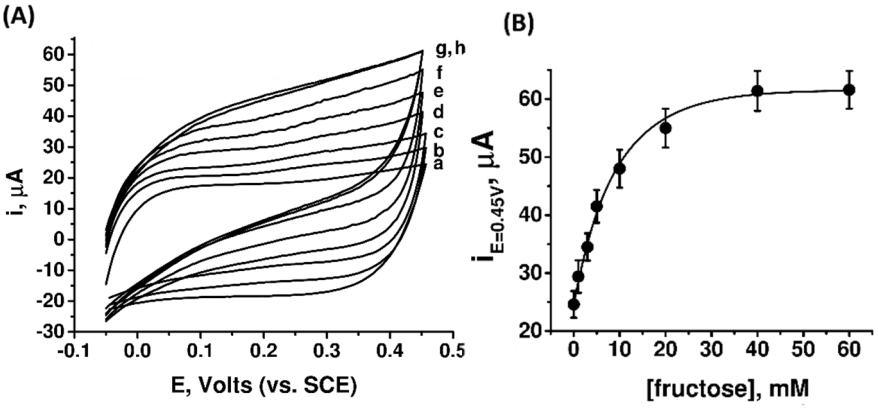

Figure 5.2 (A) CVs corresponding to direct electron transfer bioelectrocatalytic anodic currents obtained by the FDH-modified ccMNPs magnetically loaded onto a GC electrode in the presence of: (a) 0, (b) 1, (c) 3, (d) 5, (e) 10, (f) 20, (g) 40, and (h) 60 mM fructose. (B) The calibration curve depicting the amperometric responses obtained at $E = 0.45$ V vs. SCE for the various fructose concentrations.

electrolyte. Evidently, as the fructose levels in the system are elevated, higher bioelectrocatalytic anodic currents with an onset voltage slightly negative to 0.0 V vs. SCE can be observed. The calibration curve corresponding to the oxidation of the different sugar concentrations on the FDH-modified ccMNPs magnetically attached to the GC collector is depicted in Figure 5.2 (B). Using the saturation current, 62 μA, obtained at 60 mM fructose and the surface coverage of the enzyme, we evaluated the turnover rate for the DET between the FDH and the GC surface to be 780 $e^- s^{-1}$.

As one of the aims of this work is the construction of an all-DET enzymatic biofuel cell, we also tested the FDH-based anode system under O_2 saturated conditions in order to estimate the effect of the oxidizer on the anode. The results obtained demonstrate the insensitivity of the fructose oxidizing anode to the presence of O_2, showing no decrease in the catalytic current upon switching the environmental

conditions from anaerobic to aerobic in a buffer electrolyte containing 60 mM fructose, Figure 5.3. This observation correlates with the previously reported insensitivity of fructose dehydrogenase to the O_2 acceptor.[120,121] Unlike in the case of other enzymes such as GOX,[145] here O_2 mediation does not interfere with formation of the current by providing a destructive path for bioelectrocatalysis. These observations support the further design of an all-DET biofuel cell, which is operated simultaneously on both fructose and O_2.

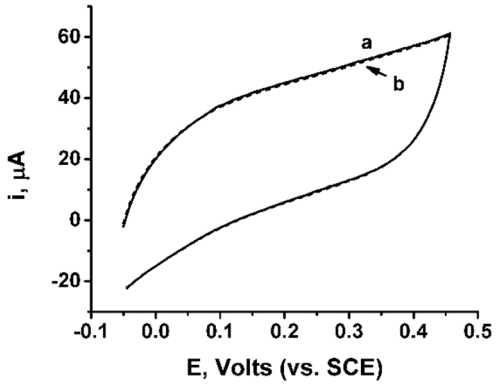

Figure 5.3 CVs showing the DET anodic currents obtained by the magnetically loaded, FDH-modified ccMNPs on a GC surface in the presence of 60 mM fructose in (a) N_2 (b) O_2 saturated electrolytes.

5.3 ON/OFF Switchable Bioelectrocatalytic Currents

Following the successful magnetically triggered generation of anodic and cathodic DET bioelectrocatalysis using the respective enzymatically modified ccMNPs, we attempted to switch the resulting currents ON and OFF. We did so by applying repetitive magnetic triggers

channeling the particles to and away from the electrode via a second magnet as depicted in Scheme 5.2. The cell is placed between two permanent magnets, M_1 and M_2, where the strength of the magnetic induction by M_2 (30x10x6 mm^3) is ca. 5.5-fold greater than that of M_1. M_1 is mounted right behind the GC collector, while M_2 can be moved perpendicular to the collector surface, at the opposite side of the cell. Therefore, the ccMNPs are exposed to a magnetic field gradient, which depends on the distance between M_1 and M_2. When M_2 is placed far enough from the cell, the enzyme-coated magnetic nanoparticles become firmly attached to the collector through M_1, and thus are electrically wired to the underlying surface. This facilitates a conductive path for the "ON" state, provided by the transfer of the electrons associated with the enzymatic transformations, leading to the generation of DET bioelectrocatalytic currents. Contrarily, upon shortening the distance between M_2 and the cell, the stronger attraction of the ccMNPs to this magnet triggers their detachment from the GC collector and accumulation at the opposite side of the cell, electrically and

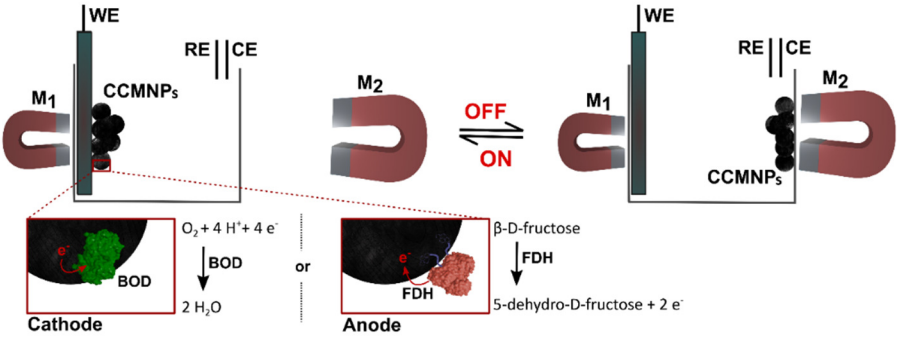

Scheme 5.2 An illustration of the magnetically assisted loading/removal of the catalytic ccMNPs from an electrode surface for the generation of direct electron transfer bioelectrocatalytic anodic or cathodic currents using FDH and BOD as the enzymatic biocatalysts, respectively.

.

electrochemically isolated from the collector. This defines the "OFF" state in which no bioelectrocatalytic response should be observed. The distances between M_1 and M_2 were controlled by a slide bar that is shown in detail in Appendix A.6.

5.3.1 Anodic and Cathodic Switches Controlled by an External Magnetic Field

By repeatedly cycling the system between the "ON" and "OFF" states, a magneto-assisted switchable DET bioelectrocatalysis was obtained for both fructose oxidation, Figure 5.4, and O_2 reduction, Figure 5.5. The cyclic voltammograms plotted in Figures 5.4 (A) and 5.5 (A) show the repetitive bioelectrocatalytic currents in the "ON" states with the respective substrates present in the electrolyte, curves (a). For comparison, the "ON" state is also depicted in the absence of fructose or oxygen, respectively, curves (c). Here, the capacitance of the ccMNPs is still evident, but no bioelectrocatalysis takes place. Curves (b) show the "OFF" state of the system, where the ccMNPs are held at the opposite side of the cell by M_2. Under this condition only the capacitance of the blank GC current collectors is evident. The maximal measured currents are plotted for FDH at 0.45 V in Figure 5.4 (B) and for BOD at 0.0 V in Figure 5.5 (B). The successful repetitive switches are evident from the persistent differences in the current densities obtained for the "ON" and "OFF" state in both systems. As can be seen, the switching does not fully reproduce the exact amperometric responses. In both cases, the recovery of the initial bioelectrocatalytic current after 6 ON/OFF cycles corresponds to 92±1%, and upon the application of several tens of cycles, the bioelectrocatalytic currents diminished below 50% of their initial values. The gradual decrease may be

explained by small mass losses of ccMNPs with every cycle by precipitation of disintegrated ccMNPS or displacement from particles in cracks of the setup disconnected from the current collector. The losses accumulate due to the magnetically induced repetitive motion of the same particles and can affect the current outputs more than the loss of enzymatic activity over the same time scale. Some minor variance in reproducibility can also be attributed to changes in the macroscopic rearrangement of the magnetized assembly on the surface, i.e. the occasional formation of magnetized "rod-like clusters" in comparison to more evenly distributed assemblies, leading to varying pathways of electron flow, which can lead to small differences in DET output. The loss of ccMNPs due to displacement during the relocation of particles might be further studied and could be potentially minimized with more precise fitting of the cell wall and working electrode widths and

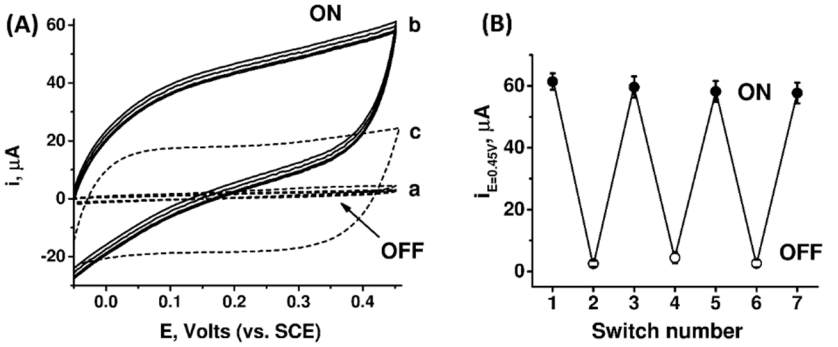

Figure 5.4 (A) CVs of repeatedly switching ON/OFF anodic biocatalysis using FDH-modified ccMNPs on GC: (a) M_2 activated - OFF state in the presence of 60 mM fructose, (b) M_2 deactivated - ON state in the presence of 60 mM fructose. Curve (c) shows, for comparison, the ON state in the absence of fructose. (B) The amperometric responses of the system at E = 0.45 V vs. SCE upon the ON/OFF switching and the resulting loading/releasing of the FDH-modified ccMNPs from the GC electrode in the presence of fructose.

automated instead of manual switching of the magnetic field gradient. It is important to note that the repetitive re-establishment of the "OFF" state indicates the easy detachment of the particles from the electrode and therefore minimizes the potential long-term effects of biofouling or residues of biocatalyst on the current collector.

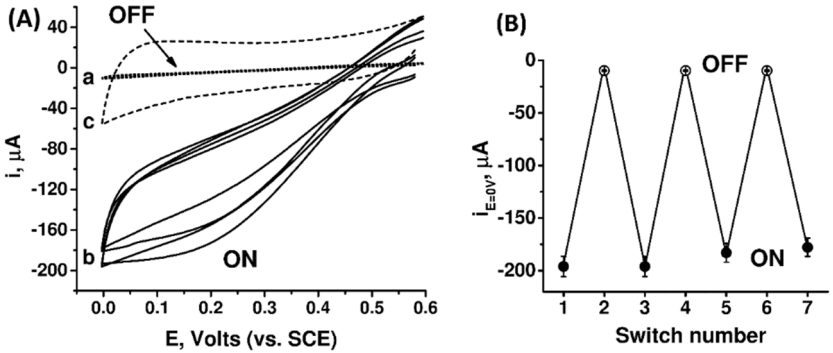

Figure 5.5 (A) CVs of repeatedly switching ON/OFF cathodic biocatalysis using BOD-modified ccMNPs on GC: (a) OFF state in the presence of an O_2-saturated buffer, (b) ON state in the presence of an O_2-saturated buffer. Curve (c) shows, for comparison, the ON state in the presence of a N_2-saturated buffer. (B) The amperometric responses of the system at E = 0 V vs. SCE upon the ON/OFF switching and the resulting loading/releasing of the BOD-modified ccMNPs from the GC electrode in the presence of O_2.

5.3.2 Applicability to Different Current Collectors

As a part of this study, we were interested in the applicability of the magneto-assisted switchable DET bioelectrocatalysis to current collectors other than glassy carbon. In a comparative set of experiments, we tested the FDH- and BOD-functionalized ccMNPs on Au-film coated glass and on indium tin oxide, ITO, slides. Figure 5.6 and Figure 5.7 present the amperometric responses corresponding to the ON/OFF anodic and cathodic bioelectrocatalytic switches obtained

upon using the different conductive collectors. No significant differences were observed for the performance of the BOD-modified ccMNPs cathodic system on GC, Au or ITO. However, an approximately 250 mV shift in the onset potential of anodic biocatalytic currents was observed from ca. 0.0 V for GC to ca. 0.25 V vs. SCE for Au as well as ITO in the presence of 60 mM fructose. As the nominal geometrical area of all tested conductive collector layers was approximately the same, we suspect that the lower overpotential on GC may be attributed to the stronger interactions provided by this collector to the 1-pyrenemethylamine coating used in the case of the FDH-modified ccMNPs. The use of this substance was observed to increase the electron transfer wiring efficiency between the FAD center of the enzyme and the collector, and we suspect that due to its own interactions, i.e. π-π stacking, with the carbonaceous underlying collector, a more facile direct charge transfer was achieved in this case.[160] Accordingly, we have selected to focus only on GC-based systems for further experiments within this study. Nevertheless, the results indicate that in all cases the magnetically triggered DET switching was effective, highlighting the versatility of the method towards different electrode materials.

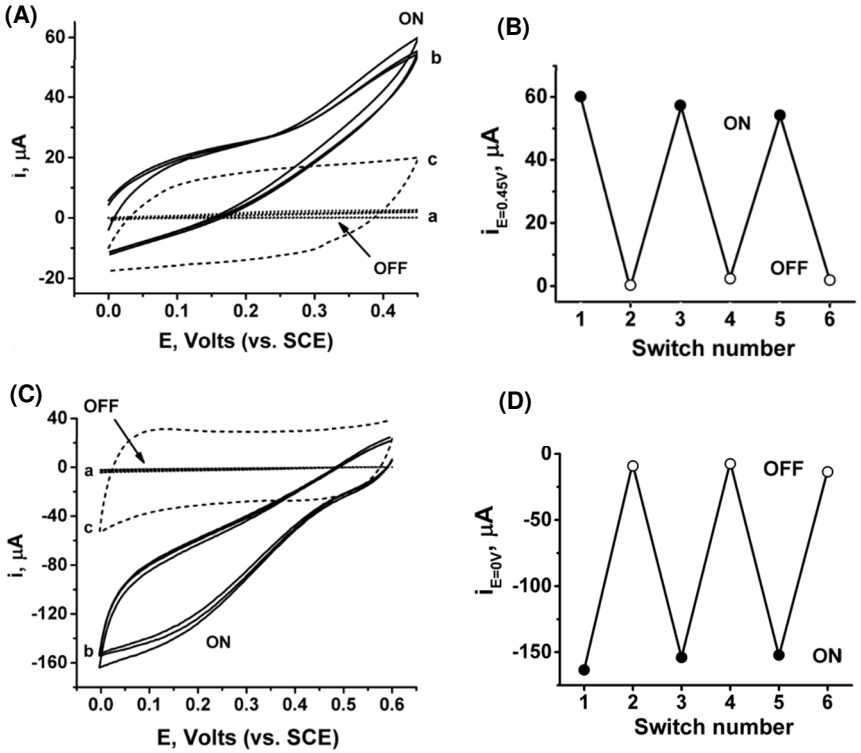

Figure 5.6 (A) CVs of repeatedly switching ON/OFF anodic biocatalysis using FDH-modified ccMNPs on ITO: (a) M_2 activated - OFF state in the presence of 60 mM fructose, (b) M_2 deactivated - ON state in the presence of 60 mM fructose. Curve (c) shows, for comparison, the ON state in the absence of fructose. (B) The amperometric responses of the system at E = 0.45 V vs. SCE upon the ON/OFF switching and the resulting loading/releasing of the FDH-modified ccMNPs from the ITO electrode in the presence of fructose. (C) CVs of repetitively switching ON/OFF cathodic biocatalysis using BOD-modified ccMNPs on ITO: (a) OFF state in the presence of an O_2-saturated buffer, (b) ON state in the presence of an O_2-saturated buffer. Curve (c) shows, for comparison, the ON state in the presence of a N_2-saturated buffer. (D) The amperometric responses of the system at E = 0 V vs. SCE upon the ON/OFF switching and the resulting loading/releasing of the BOD-modified ccMNPs from the ITO electrode in the presence of O_2.

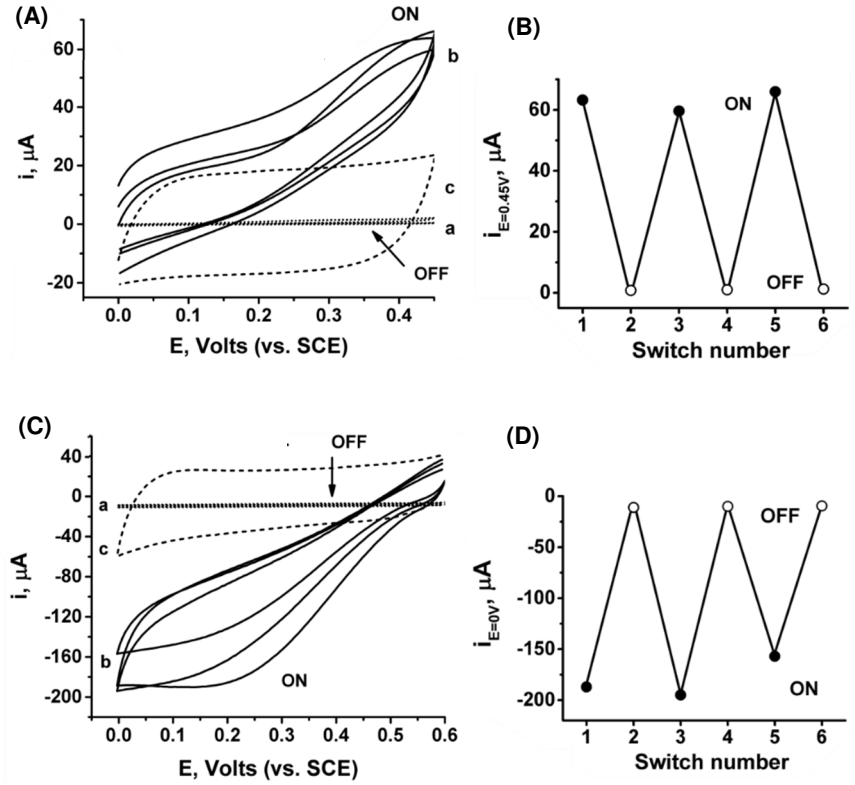

Figure 5.7 (A) CVs of repeatedly switching ON/OFF anodic biocatalysis using FDH-modified ccMNPs on Au electrode: (a) M_2 activated - OFF state in the presence of 60 mM fructose, (b) M_2 deactivated - ON state in the presence of 60 mM fructose. Curve (c) shows, for comparison, the ON state in the absence of fructose. (B) The amperometric responses of the system at E = 0.45 V vs. SCE upon the ON/OFF switching and the resulting loading/releasing of the FDH-modified ccMNPs from the Au electrode in the presence of fructose. (C) CVs of repetitively switching ON/OFF cathodic biocatalysis using BOD-modified ccMNPs on Au electrode: (a) OFF state in the presence of an O_2-saturated buffer, (b) ON state in the presence of an O_2-saturated buffer. Curve (c) shows, for comparison, the ON state in the presence of a N_2-saturated buffer. (D) The amperometric responses of the system at E = 0 V vs. SCE upon the ON/OFF switching and the resulting loading/releasing of the BOD-modified ccMNPs from the Au electrode in the presence of O_2.

5.3.3 Magnetically Induced Biofuel Cell Operation

Bringing together the promising results that were acquired separately for the anode and the cathode, we constructed an all-DET biofuel cell whose enzymatic assemblies could be selectively added to, or removed from the conductive collectors through magnetic triggers. A setup similar to the one used for the single electrode measurements, Scheme 5.2, was employed. In this case, however, two cuvettes were combined, sharing one perforated wall, thus allowing a seamless electrolyte flow throughout all parts of the electrochemical cell. The all-DET biofuel cell with a FDH-modified ccMNP anode and a BOD-modified ccMNP cathode was exposed to an oxygen-saturated electrolyte containing 60 mM of fructose. Figure 5.8 depicts the responses recorded for variable external resistances upon magnetically assisted attachment of the nanoparticles to the GC support. The polarization

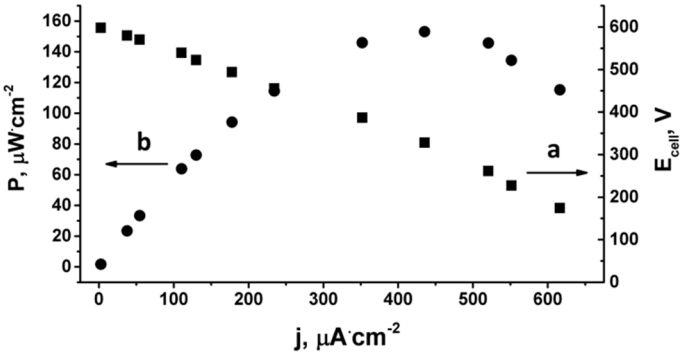

Figure 5.8 Discharge characteristics of the all-direct-electron-transfer FDH-modified ccMNPs // BOD-modified ccMNPs biofuel cell in the presence of 60 mM fructose in O_2-saturated electrolyte: (a) polarization curve showing the cell voltage, and (b) the power density of the cell. The cell was discharged versus different constant resistors in the ON state (upon magnetically loading the particles onto the GC collectors).

profile, curve (a), indicates that the discharge voltage of the cell remained higher than a cut-off voltage of 0.2 V up to a current density of ca. j = 550 μA cm^{-2}. Also, the open circuit potential corresponded to ca. E_{OCP} = 0.6 V, in agreement with the difference between the onset potentials observed for the bioelectrocatalytic processes at the cathode and the anode. The power density characteristics, curve (b), showed a peak at j = 440 μA cm^{-2} corresponding to P_{max} = 153 μW cm^{-2}. Compared to other DET based biofuel cells, this power output density is considered moderately high.[31] Furthermore, through the use of the magnetic switching methodology and by maintaining both the fructose fuel and the O_2 oxidizer in the system, we were able to selectively turn ON and OFF the power generation in the cell, Figure 5.9. The relatively short timescale and planar migration characteristics of the enzyme-coated magnetic nanoparticles across the cell upon the approach or removal of magnet M_2 avoid the mixing of the two populations of anodic and cathodic nanoparticles, thus limiting the chance of self-discharge. This allows the design of the biofuel cell in a single

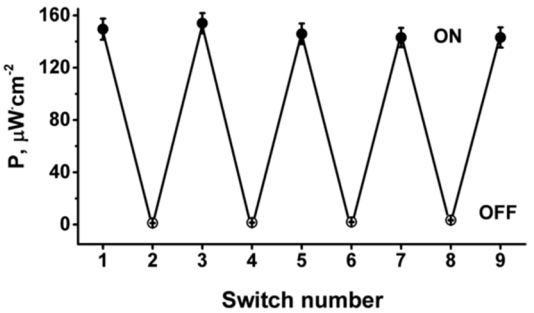

Figure 5.9 Power responses of the biofuel cell towards the applied ON/OFF magnetic switching and the resulting loading/releasing of the bioactive components from the collectors.

compartmentalized unit, minimizing potential voltage losses due to membrane resistance effects during the passage of a current.

5.4 A Magnetically Controllable Dually Cascaded EFBC

The promising results of magneto-induced switching of the EBFC led us to extend this concept towards multi-enzymatic architectures. Bringing together cascaded electron transfer pathways discussed in Chapters 3 and 4 with our concept of magneto-assisted DET switching could substantially broaden the range of applicable fuels and corresponding enzymes. To this end, we designed a similarly functioning cell yet operated by enzymatic cascades, which facilitated a multi-substrate consumption in both aerobic and anaerobic environments. For this purpose, we interacted one batch of ccMNPs with both FDH and INV enzymes, and a second batch of ccMNPs with a mixture of BOD and CAT, as described in Appendix A.3. As all reactions occur

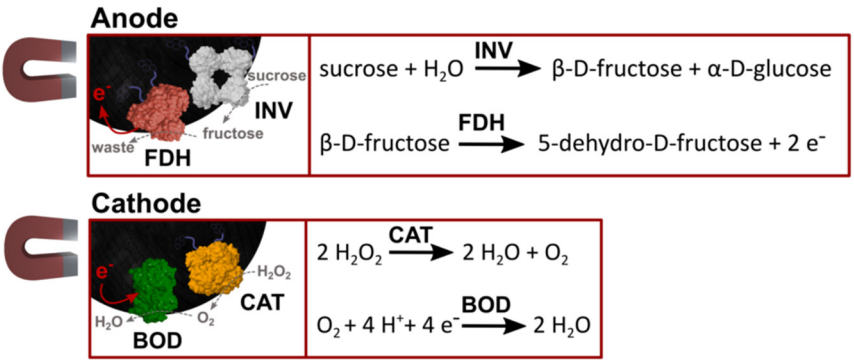

Scheme 5.3 Schematic illustration of the biofuel elements employed in the fabrication of an all-direct-electron-transfer biofuel cell operated through dual enzymatic cascades: FDH/INV-modified ccMNPs // BOD/CAT-modified ccMNPs.

by DET, the bioelectrocatalytic reactions are presumed to proceed as shown in Scheme 5.3.

The FDH/INV and the BOD/CAT bi-enzyme-modified nanoparticles were introduced into the cell and loaded onto the GC current collectors by the external magnetic field gradient. Through the INV-catalyzed splitting of sucrose to fructose and glucose, and the CAT-catalyzed disproportionation of H_2O_2 to water and oxygen, we were able to generate electrical power in the presence of sucrose under anaerobic conditions. The oxygen oxidizer was formed within the N_2-purged electrolyte through the enzymatic CAT reaction at the cathode. The performance of this all-DET dual enzymatically cascaded and magnetically induced biofuel cell was analyzed by recording its discharge characteristics in the presence of 200 mM sucrose in a N_2-saturated electrolyte containing 20 mM H_2O_2, Figure 5.10. The polarization curve shows a decent stability of the cell at current densities up to 170 μA cm^{-2}. The power density reaches its peak around 47 μW cm^{-2} at a current density of 130 μA cm^{-2} (external resistance of 150 kΩ).

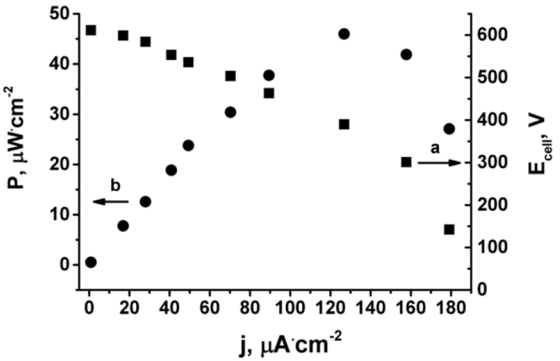

Figure 5.10 Discharge characteristics of the cell in the presence of 200 mM sucrose in N_2-saturated electrolyte containing 20 mM H_2O_2: (a) polarization curve showing the cell voltage, and (b) the power density of the cell.

The successful ON/OFF magnetic switching of the cascaded biofuel cell was also demonstrated, Figure 5.11. The power output could be reversibly shut down and reinstated using the same batches of modified ccMNPs with no apparent residues or accumulation of particles on the electrode surfaces during the "OFF" states. Furthermore, we could not detect mixing of cathodic and anodic particles during the transition across the cell.

These results demonstrate and emphasize the general applicability of magneto-assisted switchable biofuel cells to harness energy from different biomass sources, and the possibility to control them through external triggers.

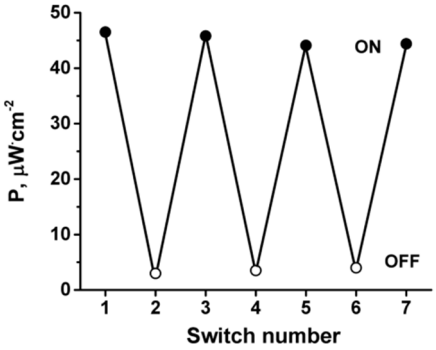

Figure 5.11 Power responses of the biofuel cell towards the applied ON/OFF magnetic switching. The cells were transiently discharged at the resistances corresponding to their maximal power outputs.

5.5 Potential Applications

We regard the magnetizable EBFC systems as promising devices allowing control by a non-invasive external field. Enzyme modified ccMNPs can be utilized to support an ON/OFF-switching mechanism

as well as in situ replacement of active electrode material. These nanoparticles pose an attractive medium to transport an active part of the cell's circuit in and out of a permanently installed cell body. Here, we achieved magnetically assisted switchable heterogeneous electron transfer. A fully reversible electrical contact between the active centers of the ccMNP adsorbed enzymes and electrochemical transducer surfaces was demonstrated, supporting simultaneous switching of anodic and cathodic reactions.

6 A Reenergizable Enzymatic Biofuel Cell

One of the main challenges in establishing EBFCs as alternative power sources in portable/medical electronic devices is the degradation of the biological components and therefore the limited durability of discharge. Here, we extend the previously introduced magnet-based method to switch bioelectrocatalysis ON and OFF to prolong the lifetime of an enzymatic biofuel cell by periodically renewing the active material. The reenergization process turns the enzymatic biofuel cells into "externally rechargeable" devices, extending their usage beyond the conventional single full discharge timeframe. Alternative approaches found in literature, long-term performance and future implications reenergizable biofuel cells are discussed.*

6.1 Towards High-Durability Enzyme Electrodes

Limited long-term activity of enzymes is one of the main obstacles hindering EBFCs entering the market. Efforts to extend the durability of these systems have paid off over the last years in terms of optimized conditions ensuring maximum enzyme stability when immobilized on electrodes. For example, an advanced system was reported by Okuda et al. employing an anode supporting DET with modified glucose dehydrogenase that showed 20% loss after 72 hours of constant operation.[161] The decrease in the signal response was attributed

* This chapter contains parts of the publication K. Herkendell, A. Stemmer, and R. Tel-Vered, "Reenergizing enzymatic biofuel cells through magnetically assisted induction of direct electron transfer pathways", *submitted*.[148]

to irreversible denaturation of the enzyme or reversible apo-enzyme formation.

Whereas most reported EBFCs do not document their long-term performance, others state the lifetime by testing either the system's or the single electrode's activity by spot-checking the performance and applying load on a periodical basis. The lifetime values of these systems are typically reported to be several days and can reach up to 28 days.[162-164] In these cases the electrodes are often stored in buffer at 4°C and tested every 24 hours, distorting the comparison of the durability to lifetimes under constant discharge.

Few studies exist that document EBFC performance under long-term operation. For a continuous discharge of a biofuel cell with an anode modified by GOX in conjunction with an air breathing cathode, Kim et al. reported relatively stable currents for a duration of 16 hours and storage stability of 143 days.[165] Other reports show half-life values ranging between 2 and 30 hours[164-170] with a few higher exceptions.[28,171,172]

EBFCs based on DET often display superior durability compared to mediated systems as they do not suffer from loss of mediator molecules.[81] This issue also is critical for potentially implantable EBFCs, as leakage of electrode material or high-frequent replacement surgery are not acceptable. Nevertheless, first approaches towards implanting EBFCs to power small electronic devices have been successfully demonstrated in recent years.[173,174] Furthermore, already existing power sources for implantable medical devices are not flawless. Missing recharging options, insufficient long-term biocompatibility and frequent battery replacement surgery e.g. for the commonly used lithium cell open the door for more environment-compatible options.[18,175]

Despite anticipated future advances towards optimized enzyme immobilization for EBFC systems to reach maximized lifetimes of catalytic activity, nevertheless, enzymes will always have a finite lifetime originating in their delicate organic structure.

Supercapacitor-biofuel cell hybrids were recently introduced as an innovative approach to store enzymatically converted energy within a carbon nanotube matrix.[176] This concept can slow down the enzyme's deterioration, as the biocatalysts do not operate under continuous discharge. In this study, however, a constant power could be provided for only 5 days.

To extend the overall durability of a GOX / LAC operated EBFC, Reuillard et al. recently focused on the time-dependent catalytic activity of the LAC-based cathode which they identified as the bottleneck to the overall power output.[177] As the power dropped by 25% within the first hour of operation due to LAC inactivation by the gradually increasing pH, they could extend the operation by reactivating the cathode through storing it in acidic conditions. Following this methodology, the glucose-operated cell exhibited an overall power loss of only 22% after one year. However, during this time the cell was discharged at the maximum once per day for 1 hour on a non-regular basis. Thus, this approach is not suitable for permanent discharge conditions. In addition, despite the impressive recovery of the cathode, the finite stability of GOX and LAC remained.

Miyake et al. introduced an interesting approach for prolonging the net lifetime of a biofuel cell through assembly of a miniature flow cell stack of EBFC chambers that are sequentially and automatically opened and exposed to the substrate solution.[178] The opening of the consecutive chamber was triggered by an external magnetic field, as the covers sealing each chamber were magnetized. In this setup, a new chamber was opened approximately every 15 hours, thus extending

the operation time of the system by that time per stacked chamber. Concerning the potential to upscale this approach in terms of lifetime, the space taken by the stacks will clearly be the limiting factor.
In Chapter 5, we introduced biofuel cells that enable magnetically switchable and fully reversible electron transfer pathways between the active centers of the ccMNP-adsorbed enzymes and electrochemical transducer surfaces, simultaneously for anode and cathode. In the following sections, we extend this methodology to long-term fuel cell operation under load by reenergizing the cell via replacement of the active electrode material guided by suitable magnetic fields.

6.2 Renewing Active Electrode Material via an External Magnetic Field

The enzyme-modified ccMNPs were further used to energize biofuel cells. As previously shown, the bioelectrocatalytically active enzyme-modified ccMNPs can be magnetically detached from the surface and relocated to an electronically insulated region by changing the magnetic field gradients. We wanted to utilize this quality to trigger reenergization cycles of the fuel cell by replacing the active material, as illustrated in Scheme 6.1. The cell is loaded with anodic and cathodic enzymatically modified ccMNPs with the help of M_1, step (1). The cell is then discharged against an external load as long as the enzymes remain sufficiently active and immobilized, step (2), characterized by the output voltage staying above a cut-off threshold. The reenergization process is subsequently activated by approaching M_2, as the catalytically exhausted ccMNPs are transported across the cell and attached to a temporal “transit station” surface, step (3). As the last step, the used particles and M_2 are removed, step (4), and fresh

ccMNPs are loaded on the electrodes as the cycle starts over. Depending on the time-interval after which the MNP components are replaced, the system is rendered free from biofouling or enzyme instability issues. For the described system we determined a continuous discharge duration that did not exceed 20 hours until cut-off.

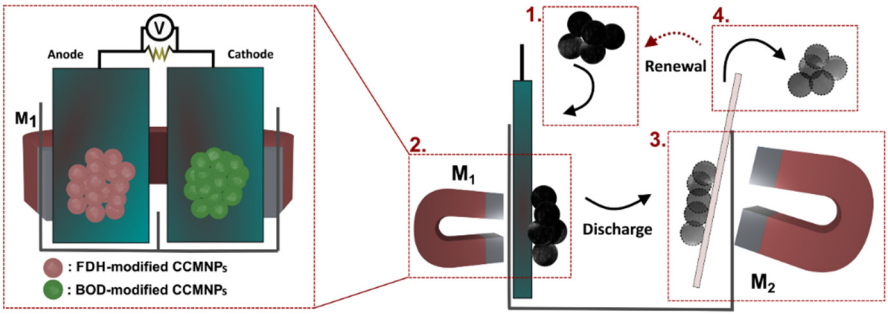

Scheme 6.1 An illustration of the all-direct-electron-transfer FDH-modified ccMNPs // BOD-modified ccMNPs biofuel cell whose biocatalytic components are being loaded/removed from the respective base current collectors using magnetically assisted methodology. The renewal of the active components, extending the operation of the biofuel cell, is followed by the steps: (1) Introducing the FDH-modified ccMNPs and BOD-modified ccMNPs respectively to the two directly linked anodic and cathodic cuvette compartments under the magnetic field induced by M_1. (2) Discharging the cell under a constant external load. (3) Removal of the inactive ingredients through their magneto-assisted transport onto an inert Teflon™ surface using M_2 and (4) their displacement from the cell. A further distancing of M_2 while introducing fresh bioactive components to the cell fully regenerates the discharge power outputs.

6.3 Long-Term Operation of an All-DET Enzymatic Biofuel Cell

To test this protocol, we have discharged the FDH- and BOD-modified ccMNPs biofuel cell to a cut-off voltage of E_{cell} = 200 mV at a relatively high rate corresponding to 80% of the maximal observable power output (R = 39 kΩ). During the discharge, we periodically verified that

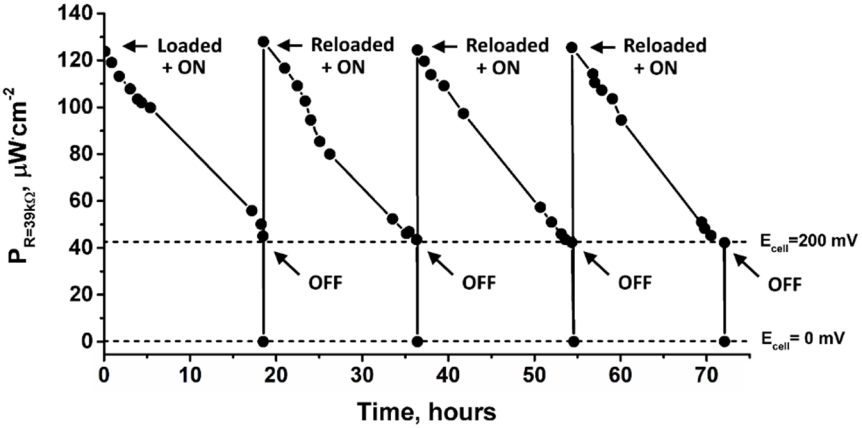

Figure 6.1 Repetitive discharge/charge cycles demonstrating the magnetically assisted reenergizing of the all-direct-electron-transfer FDH-modified ccMNPs // BOD-modified ccMNPs biofuel cell. The power of the cell was repeatedly regenerated using the procedure in (A). Discharge was performed at R = 39 kΩ, corresponding to 80% of the maximal power output.

the fructose levels in the system remained saturated, and that a constant flow of O_2 was continuously streamed over the electrolyte. As can be seen from Figure 6.1, following ca. 18.5 hours of discharge, the cell power dropped to slightly above 40 μW cm^{-2}, which correlates with E_{cell} = 200 mV. Through the magnetically assisted removal of the enzyme-modified ccMNPs and by spectroscopically assaying their enzymatic activity, we estimate that the discharge to this cut-off voltage accounts for an activity drop in excess of 65% for both FDH and BOD. To reenergize the cell, the replacement steps described before were applied without disconnecting the external load. We released the nanoparticles from the GC collector using M_2, and simultaneously magnetically channeled them onto mobile slides that had been mounted at the opposite walls of the cuvettes-based cell. The displacement process is shown in Scheme 6.2. After removing the ccMNPs-loaded

slides from the cell and washing off the particles of their surface, the clean slides were reinserted to the cell. At the same time, M_2 was removed from the vicinity of the cell and finally, fresh suspensions of the anodic and cathodic enzyme-modified nanoparticles were introduced near the corresponding GC surfaces, resulting in their magnetized attachment. The timescale of the replacement process was approximately 20-30 seconds. This time interval might be significantly shortened through the use of an automated system. Figure 6.1 presents the prolonged discharge profile of the biofuel cell upon

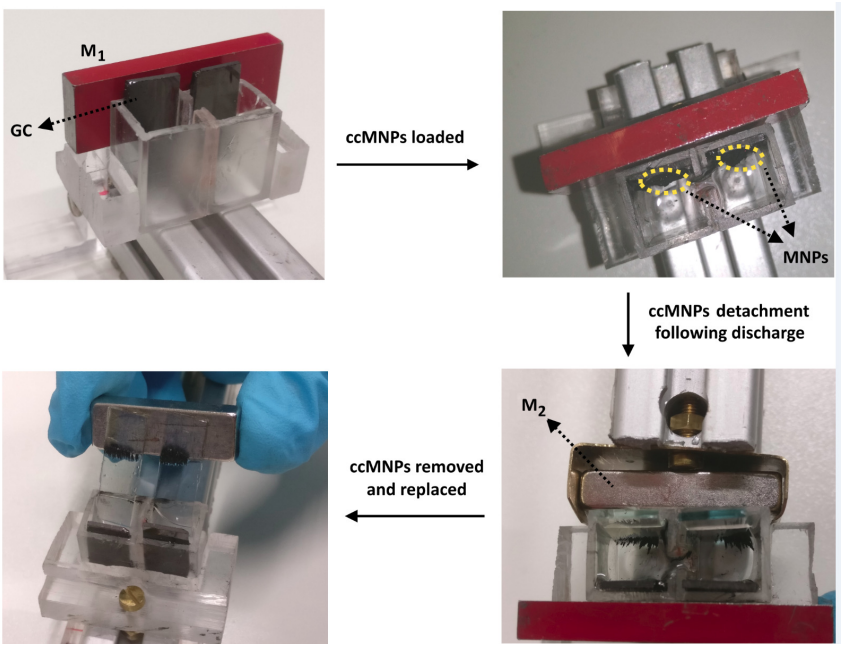

Scheme 6.2 Images of the exchange process of active material with the help of M_1 and M_2. In this setup, GC slides embody the current collectors inside the anodic and cathodic connected half-cell cuvettes, and glass slides are used for the displacement of the ccMNPs from the cell. To permit better view, the electrode connections are not shown.

repeatedly reenergizing it at a cut-off voltage of E_{cell} = 200 mV for several cycles. Evidently, following the magneto-assisted release of the enzyme-modified ccMNPs from the electrode surfaces at the cut-off potential, the cell voltage dropped in each cycle to approximately 0 V, marked by the "OFF" state. This observation implies the full removal of the particles from the surface, as at this stage the voltage was measured between two identical bare GC electrodes. Similar power discharge curves were obtained for the consecutive reenergizing processes with apparent variations attributed to minor room temperature changes and the structural effects exerted by the magnetic field mentioned earlier. This methodology is shown for 4 cycles, and can be seamlessly extended as no signs of non-removed particles could be observed.

6.4 Implications towards Future Applications

Efforts to establish EBFCs as lasting alternative power sources solutions for implants or low-power portable devices might lead to advantageous outcomes in terms of biocompatibility, toxicity, cost efficiency and environmental compatibility. Permanently installed miniaturized cells with in and outlets for fuel and active material supply might be designed and controlled via non-invasive magnetic controls. A complementary successful implementation of the methodology in activating enzymatic cascades further highlights the possibilities to exploit a broad range of fuels/oxidizers, and to harvest electrical energy from alternative biomass sources.

The presented on-demand magneto-switchable fuel cell setup enables the regeneration of electrocatalytically bioactive substances. The successful ON/OFF switching and long-term operation with a renewal cycle of 18.5 hours is demonstrated on a fructose/oxygen cell based on

FDH- and BOD-functionalized magnetic nanoparticles. The successfully demonstrated reenergization process and the resulting minimization of degradation effects, such as biofouling or enzyme stability problems significantly broaden the possibilities to integrate EBFC systems in various applications.

7 Summary and Future Perspectives

This work presented novel concepts to advance the applicability of biofuel cells in powering electronic devices. We discussed challenges and major drawbacks of current enzymatic fuel cells, including single-enzyme electrodes processing only a single component in complex biofuels, the insufficient exploitation of chemically stored energy of different substrate molecules, the kinetic bottleneck imposed by the cathodic oxygen reduction, and the limited operational lifetime of enzymatically modified electrodes. Within this thesis we proposed methodologies that offer possible solutions or bypasses of these issues and demonstrated these concepts on a set of exemplary saccharide/oxygen enzymatic biofuel cells.
Important recurring elements throughout this work include (i) the successful electrical wiring of bio-nano hybrid building blocks, (ii) the implementation of enzymatic cascades, and (iii) the design and actuation of switching mechanisms for the operation of the cells.

(i) Bio-nano hybrids were synthesized on both mesoporous carbon nanoparticles and carbon coated magnetic carbon particles. While the former supported mediated electron transfer upon deposition on a glassy carbon surface, the latter exhibited direct electron transfer when attached to various current collectors. The first-mentioned building blocks were assembled by mediator unit entrapment inside the mesoporous matrices and their subsequent capping by redox enzymes. This allowed the generation of electrically wired assemblies facilitating a variety of efficient enzymatic transformations for the generation of electrical current and power. The core cathodic hybrid

structures consisted of the oxygen reduction biocatalyst bilirubin oxidase mediated by pore-entrapped 2,2′-azino-bis(3-ethylbenzothiazoline-6-sulfonic acid) molecules. The core anodic hybrid structures involved the redox enzymes fructose dehydrogenase and glucose oxidase mediated by ferrocenemethanol or tetrathiafulvalene.

The basic components utilized for the generation of direct electron transfer on the carbon coated magnetic nanoparticles involved the redox enzymes bilirubin oxidase (cathodic assembly) and fructose dehydrogenase (anodic assembly).

(ii) Enzymatic cascades were implemented for constructing mediated and direct electron transfer anodic and cathodic half-cells. The cathodic half-cell cascade incorporated a combined catalase and bilirubin oxidase assembly that enabled the disproportionation of hydrogen peroxide to water and oxygen by catalase, with the subsequent BOD-catalyzed reduction of the generated oxygen to water. The anodic half-cell cascades were based on the hydrolysis of sucrose via invertase to fructose and glucose as intermediate products. These product molecules were subsequently oxidized in a parallel cascading step via fructose dehydrogenase and glucose oxidase to yield the anodic bioelectrocatalytic currents. The cascaded path using glucose oxidase involved an additional step of interconversion of the anomers of glucose catalyzed by the enzyme mutarotase. To the best of our knowledge we have presented the first biofuel cell that operates with immobilized cascades for both half-cell reactions. This was realized for enzymatic biofuel cells based on direct as well as mediated electron transfer.

(iii) The cells were designed to respond to two types of switching mechanisms: The bioelectrocatalytic currents could be switched ON/OFF by an external magnetic field, and multi-enzyme responsive electrodes allowed switching between different fuels and between aerobic

and anaerobic operation. To realize the magnetic switch, we took carbon nanoparticles with a magnetizable core and coated them with the required enzymes. External magnetic field gradients allowed us to selectively translocate them onto electrodes to initiate the "ON"-state or to remove them from the electrodes to induce the "OFF"-state. Whenever magnetically loaded onto a current collector and in the presence of the respective substrates, the enzyme-modified particles enabled direct electron transfer pathways between the redox centers of the enzymes and the conductor supports.
Multi-enzyme modified electrodes allowed biofuel cells to operate with sucrose, glucose, or fructose and the use of oxygen and/or hydrogen peroxide as an internal source of O_2. This type of enzymatic biofuel cell can also be repeatedly switched between aerobic and anaerobic conditions.

Regarding the challenges in the field of enzymatic biofuel cells mentioned at the beginning of this chapter, we conclude that combining several cascading enzymatic reactions on electrodes broadens the spectrum of fuels that can be consumed for the generation of electrical power. We highlight the potential use of mixed-fuel biomass as alternative energy resources to nowadays fuel cells. In this study, we have implemented nano-scaled mesoporous supports to build cascaded electrodes serving as anodic and cathodic elements of a multi-substrate-operated biofuel cell. Whereas the mesoporous carbon nanoparticle matrices used in the cascaded assemblies performed efficiently, it should be emphasized that the reported design is not limited to this specific substrate and may be implemented in conjunction to other porous conducting materials as well.
Furthermore, one can conclude that enzymatic cascades enable a deep oxidation of complex substrate molecules and therefore convert the

chemically stored energy more efficiently. The anodic enzymatic cascade involving invertase, mutarotase, glucose oxidase, and fructose dehydrogenase efficiently demonstrated a four-electron oxidation of sucrose molecules by two parallel-mediated enzymatic redox reactions performed by fructose dehydrogenase and glucose oxidase on the mesoporous carbon nanoparticle matrix. Additionally, we demonstrated the successful cascaded oxidation of sucrose without additional mediator units via invertase and through the direct electron transfer features of fructose dehydrogenase on carbon coated magnetic nanoparticles. Based on these results, an even deeper oxidation of sucrose might be envisaged by adding enzymatic cascade steps to further oxidize the waste products gluconolactone and 5-dehydro-D-fructose. Alternative enzymatic cascades may also be introduced in an attempt to achieve a deeper oxidation in the system.

Interesting future directions include mimicking the interplay of the sequential enzymes within cascades as found in nature, so called metabolons.[179] Biofuel cell efficiencies might be optimized by channeling an intermediate product towards the next cascade step and by minimizing the distances between the active sites of sequential enzymes.

One also can conclude that the enzymatically catalyzed transformation of hydrogen peroxide to oxygen exploits the substance as an internal source of oxygen for the cathodic biofuel cell reduction reaction. This approach can circumvent the restricted solubility and diffusion barriers of oxygen in electrolytes that often cause the cathode to be the power-limiting element in the enzymatic biofuel cells. In the fuel cell demonstrated, peak power densities were elevated from 40 μW cm^{-2} with oxygen as the single oxidizer source to 150 μW cm^{-2} using hydrogen peroxide as the single oxidizer source and to more than 240 μW cm^{-2} upon the use of both oxidizer sources combined. The observed compatibility of the cell with the sole presence of hydrogen peroxide

enabled its operation in anaerobic environments. To verify this, we have repeatedly switched the aerobic and anaerobic conditions, and observed a fully potent performance by the cell in both environments. The possibility to efficiently deliver electric power in both O_2 rich and O_2 free environments significantly widens the range of potentially exploitable biofuel-containing environments. The concept and design of the reported biocathodes will hopefully trigger the construction of further devices operating in O_2-independent environments.

Finally, to bypass the limited operational lifetime of enzymatically modified electrodes, we suggested a concept based on nanoparticle-enzyme conjunctions to control bioelectrocatalysis. This methodology was used to reenergize enzymatic biofuel cells through the assistance of external magnetic triggers, turning them into "externally-rechargeable" alternative power sources and extending their discharge lifetimes beyond the conventional single time use. The enzymatic functionalization of magnetic nanoparticles enabled direct electron transfer when magnetized to different current collectors and, respective to the enzymes and substrates employed, supported the generation of either anodic or cathodic currents. These results led to the assembly of a biofuel cell based on fructose dehydrogenase and bilirubin oxidase functionalized carbon coated magnetic nanoparticles, exhibiting an on-demand magneto-assisted switchable ON/OFF production of power. The feasibility of this switching allowed an implementation of the setup for a periodic regeneration of the electrocatalytically bioactive components of the cell. Using permanent magnets as binding and releasing elements, the anodic and cathodic layers were repeatedly refreshed, leading to a prolonged sustainable operation of the all-direct electron transfer biofuel cell assembly. In the demonstrated long-term experiment, one cycle of discharge of the cell under a constant external load lasted ca. 18.5 hours. The cycle duration was defined by

the operation time above a cut-off voltage of 200 mV, which was eventually reached due to the gradual enzymatic activity decrease. In the following exchange process, the exhausted active material was relocated by magneto-assisted transport onto an inert mobile surface to be removed from the cell. Restoring the initial magnetic field and introducing fresh bioactive components to the cell fully regenerated the discharge power outputs.
This replacement strategy for biodegraded components turns the enzymatic biofuel cell into a reusable alternative energy resource. The methodology is demonstrated to be versatile in terms of the different electrode materials used, composition of the enzymes (fuels and oxidizers), and the discharge conditions applied. The full reversibility of the switching and the replacement methodology allow a bypassing of biofouling on the current collector and enzyme stability problems.

We suggest this reenergizing strategy to be implemented for future assemblies employing enzyme-modified electrodes in order to extend their operational lifetime. This specific methodology may be promising, for example, for bio-powered implanted medical devices requiring body fixation for extended durations of time. To progress this idea, the biofuel cell design could be enhanced in terms of in- and outlets for fuel and active electrode material for a permanently installed cell body. The exchange process of active material should be automated to minimize the time of power output interruption. An interesting approach to bridge the gap between two discharge cycles might be the dual use of carbon nanostructures as mobile electrical contacting supports for the enzymes and as stationary supercapacitors[176] on the electrode surface, which might enable a seamless power output of the biofuel cell.

Overall, this work contributes to the advance of a new generation of long-term operational enzymatic biofuel cells. We hope that the concepts shown will further promote the use of such systems as alternative power sources.

A Appendix

A.1 Materials

Mesoporous carbon particles (mCNP, < 500 nm, 64 Å average pore diameter, ca. 193 $m^2\ g^{-1}$),[51] carbon coated magnetic nanoparticles (ccMNPs, d = 25 nm), glassy carbon foil (GC, thickness 1 mm), indium tin oxide (ITO)-coated glass, 1-pyrenemethylamine hydrochloride, Nafion™ perfluorinated resin (aqueous dispersion), suberic acid bis(3-sulfo-N-hydroxysuccinimide ester) sodium salt, BS^3, and poly(vinylidene fluoride), PVDF, were purchased from Sigma-Aldrich. N-Methyl-2-pyrrolidinone, NMP, was obtained from ChemieBrunschwig AG. Glucose oxidase, GOX, from *Aspergillus niger* (EC 1.1.3.4), invertase, INV, from *Saccharomyces* cerevisiae (EC 3.2.1.26), catalase, CAT, from bovine liver (EC 1.11.1.6), bilirubin oxidase, BOD, from *Myrothecium verrucaria* (EC 1.3.3.5), and peroxidase from horseradish, HRP, (EC 1.11.1.7) were purchased from Sigma-Aldrich. D-Fructose dehydrogenase, FDH, from *Gluconobacter sp.* (EC 1.1.99.11) was obtained from Toyobo Enzymes. Mutarotase, MUT, from porcine (EC 5.1.3.3) was purchased from Sinus Biochemistry & Electrophoresis GmbH. Sucrose, D-(+)-glucose, and D-(-)-fructose were obtained from Sigma-Aldrich. Hydrogen peroxide was purchased from Merck. Ferrocenemethanol, FcM, tetrathiafulvalen, TTF, potassium ferricyanide, and 2,2′-azino-bis(3-ethylbenzothiazoline-6-sulfonicacid) diammonium salt, ABTS, were purchased from Sigma-Aldrich. Glassy carbon electrodes, GCE, (d = 3 mm) were obtained from PalmSens BV.

A.2 Electrode Modification with Mesoporous Carbon Particles

GCEs were polished with 1.0 µm alumina powder on a 1200 grit carbimet disk, followed by their successive polishing with 0.3 and 0.05 µm alumina powder on a microcloth pad and rinsing with ethanol and water. A 16.6 mg ml^{-1} mCNP suspension was prepared by mixing the carbon particles for 5 minutes with NMP, followed by 120 minutes sonication. Different stock mixtures were then prepared by adding one of the redox active relays FcM, TTF (anodic mediation), or ABTS (cathodic mediation) to the base suspension to yield a final concentration of 2 mM mediator molecules per matrix volume. Following sonication for 120 minutes, 50 µl of poly(vinylidene fluoride), PVDF, solution (5 wt.% in NMP) was added to each mixture and again sonicated for 20 minutes. In the next stage, 4 µl of the respective mCNP stock suspensions were applied on top of the GC surfaces, and the electrodes were left to dry for 30 minutes at 10 mbar. The dried relay-doped matrices were then covered by 1 µl of the cross-linking agent BS^3 (1 mg ml^{-1} aq.). Subsequently, McIlvaine buffer solution (pH 5.2) containing a combination of: GOX (1 mg ml^{-1}), FDH (1 mg ml^{-1}), INV (0.3 mg ml^{-1}), MUT (0.3 mg ml^{-1}) for the anodic assemblies, and BOD (2 mg ml^{-1}), CAT (1 mg ml^{-1}) for the cathodes, 5 µl per enzyme, was applied on top of the relay-doped mCNP matrix. The modified electrodes were allowed to dry at room temperature and rinsed with buffer to remove any unbound material. Where indicated, the electrodes were coated with 3 µl of Nafion™ solution (0.5 v% aq.) and left to dry at room temperature.

A.3 Enzymatic Functionalization of Carbon Coated Magnetic Nanoparticles

5 mg ml^{-1} of 1-pyrenemethylamine hydrochloride were dispersed in 5 ml water and sonicated for 10 minutes. To this solution 5 mg of ccMNPs were added, and the resulting suspension was then shaken for 30 minutes. The pyrenemethylamine-modified ccMNPs were washed with water and subsequently suspended in 200 µl MES buffer (pH 5.5, 100 mM). In the following step 100 µl of FDH solution (8 mg ml^{-1} in MES) were added, and the suspension was left for 14 hours, allowing the enzyme to adsorb on the surface of the modified nanoparticles. The resulting FDH-modified ccMNPs were magnetically collected and washed four times in MES buffer to remove all non-bound enzymes. BOD-modified ccMNPs were similarly prepared, omitting the pyrenemethylamine pretreatment stage as the BOD exhibits both stable adsorption and DET on various carbonaceous surfaces attributed to the existence of a hydrophobic pocket near its T1 Cu site.[15,51] Prior to each measurement, a 20 µl suspension containing 25 mg ml^{-1} enzyme-modified ccMNPs were introduced into the electrochemical cell.

A.4 Voltammetric Setup

Electrochemical measurements were performed using a PalmSens3 potentiostat (PalmSens BV) connected to a three-electrode setup. A KCl-saturated calomel electrode (SCE) served as reference electrode for all measurements. All error bars indicated throughout the presented results correspond to $N = 3$ experiments. None of the experiments were mechanically stirred during measurements. If not speci-

fied, all electrolytes were saturated with N_2 before measuring. Purging with gas (N_2 or O_2) was applied for a minimum of 10 minutes before each measurement.

The experiments with mCNP matrices were performed with GCE (d = 3 mm) as working electrodes and a carbon rod (d = 5 mm) as counter electrodes in a cell volume of 75 ml. McIlvaine buffer with pH 5.2 was used at 35 ± 1 °C. The CVs were taken with a scan rate of 20 mV s^{-1} unless indicated otherwise.

The experiments with ccMNPs were performed with GC, ITO or Au working electrodes with ca. 0.8x2 cm^2 dimensions that were not fully immersed in 1 ml cell volume. The footprint of the magnetically attached ccMNPs on the current collectors was 0.05 cm^2. A carbon rod (d = 2mm) served as the counter electrode. These experiments were performed in MES buffer (pH 5.5, 0.1 M) at room temperature. The CVs were taken with a scan rate of 10 mV s^{-1} unless indicated otherwise.

A.5 Assays of Enzymatic Activity

The enzymatic activity was assayed using colorimetric procedures previously reported for GOX,[51] FDH,[180] and BOD.[181]

UV/Visible spectroscopic measurements were performed on a Bio-Rad SmartSpec Plus spectrophotometer using quartz cuvettes. The amount of the catalytically active GOX immobilized on the electrodes was determined by following the O_2-mediated oxidation of glucose. To this end, the colorimetric analysis of the enzymatically generated H_2O_2 was assayed by following the HRP-mediated oxidation of $ABTS^{2-}$ to $ABTS^{\cdot-}$ at λ_{max} = 414 nm. The active surface-bound FDH was quantified by the reduction of potassium ferricyanide

(λ_{max} = 420 nm) to potassium ferrocyanide, serving as an electron acceptor in the FDH-catalyzed oxidation of D-fructose to 5-dehydro-D-fructose. The active surface-bound BOD was quantified by following the BOD-mediated oxidation of $ABTS^{2-}$ to $ABTS^{\cdot-}$ at λ_{max} = 414 nm. With the measured enzyme concentrations, the surface coverage of active enzyme on the electrodes was determined. The effective electron transfer rates of the bioelectrocatalysis, k_{et}, for the different enzymes were calculated according to Equation A.1, using the determined current densities at saturation j_{sat}.

$$k_{et} = \frac{j_{sat}}{z_e F \Gamma} \qquad \text{(A.1)}$$

The number of electrons involved in enzymatic reaction is indicated as z_e, the Faraday's constant as F and Γ being the surface coverage of the enzymes on the electrode.

A.6 Biofuel Cell Discharge and Reenergization Setup

Power output of a biofuel cell is characterized by the cell's voltage and current. The enzymatically cascaded biofuel cells were discharged versus variable external resistances using a Keithley 2000 multimeter. The polarization curves were recorded at variable external resistances between $4 \cdot 10^6$ and $8 \cdot 10^3$ Ω.The current density j_{cell} and power density P_{cell} were determined for every applied external resistor R_{ext} according to Equations A.2 and A.3 upon stabilization of the recorded cell voltage E_{cell} for the active geometrical surface area of the working electrode A_{WE}.

$$j_{cell} = \frac{E_{cell}}{R_{ext}\, A_{WE}} \qquad \text{(A.2)}$$

$$P_{cell} = E_{cell}\, j_{cell} \qquad \text{(A.3)}$$

During the long-term discharge experiments, oxygen was constantly streamed over the surface at a fixed flow rate and the electrolyte volume and the fuel concentration were kept at a steady level. The cell volume for the long-term discharge experiments was 2 ml.
The cell including the setup that was used to exchange the active material is displayed in **Scheme A.1**.

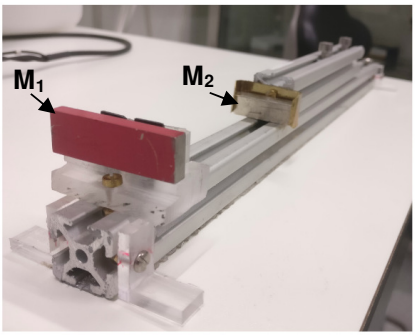

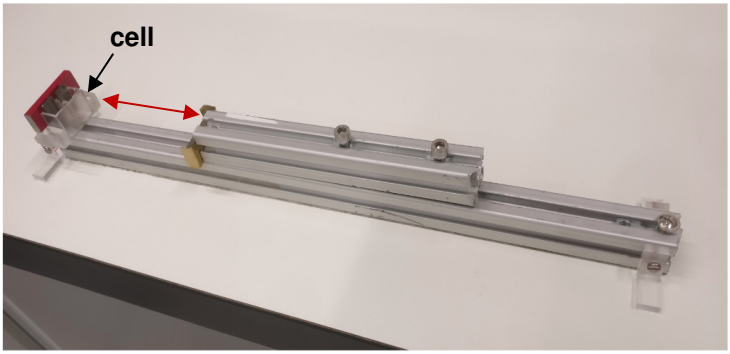

Scheme A.1 Images of the in-house built set up that controls the distance between M_1 and M_2. M_1 and the biofuel cell body are firmly installed at one end, while M_2 is connected to the adjustable slide bar.

A.7 Visualization of Enzymatic Chemical Structures

The enzymatic structures displayed were used in the schemes were visualized with Jmol: an open-source Java viewer for chemical structures in 3D. http://www.jmol.org/

Bibliography

1 M. Zhou, *Electroanalysis*, 2015, **27**, 1786-1810.

2 M. Falk, C. W. N. Villarrubia, S. Babanova, P. Atanassov and S. Shleev, *ChemPhysChem*, 2013, **14**, 2045-2058.

3 S. C. Barton, J. Gallaway and P. Atanassov, *Chem. Rev.*, 2004, **104**, 4867-4886.

4 S. A. Neto, J. C. Forti and A. R. De Andrade, *Electrocatalysis*, 2010, **1**, 87-94.

5 S. Cosnier, A. Le Goff and M. Holzinger, *Electrochem. Commun.*, 2014, **38**, 19-23.

6 E. Katz, I. Willner and A. B. Kotlyar, *J. Electroanal. Chem.*, 1999, **479**, 64-68.

7 X. Wu, F. Zhao, J. R. Varcoe, A. E. Thumser, C. Avignone-Rossa and R. C. T. Slade, *Biosens. Bioelectron.*, 2009, **25**, 326-331.

8 S. Cosnier, D. Shan and S. N. Ding, *Electrochem. Commun.*, 2010, **12**, 266-269.

9 H. H. Kim, N. Mano, X. C. Zhang and A. Heller, *J. Electrochem. Soc.*, 2003, **150**, A209-A213.

10 S. Rengaraj, P. Kavanagh and D. Leech, *Biosens. Bioelectron.*, 2011, **30**, 294-299.

11 A. Heller, *Phys. Chem. Chem. Phys.*, 2004, **6**, 209-216.

12 B. Reuillard, A. Le Goff, C. Agnes, M. Holzinger, A. Zebda, C. Gondran, K. Elouarzaki and S. Cosnier, *Phys. Chem. Chem. Phys.*, 2013, **15**, 4892-4896.

13 C. H. Kwon, S. H. Lee, Y. B. Choi, J. A. Lee, S. H. Kim, H. H. Kim, G. M. Spinks, G. G. Wallace, M. D. Lima, M. E. Kozlov, R. H. Baughman and S. J. Kim, *Nat. Commun.*, 2014, **5**.

14 K. P. Prasad, Y. Chen and P. Chen, *ACS Appl. Mater. Interfaces*, 2014, **6**, 3387-3393.

15 K. So, S. Kawai, Y. Hamano, Y. Kitazumi, O. Shirai, M. Hibi, J. Ogawa and K. Kano, *Phys. Chem. Chem. Phys.*, 2014, **16**, 4823-4829.

16 A. A. Babadi, S. Bagheri and S. B. A. Hamid, *Biosens. Bioelectron.*, 2016, **79**, 850-860.

17 M. Rasmussen, S. Abdellaoui and S. D. Minteer, *Biosens. Bioelectron.*, 2016, **76**, 91-102.

18 S. Shleev, *ChemPlusChem*, 2017, **82**, 522-539.

19 D. Sokic-Lazic, R. L. Arechederra, B. L. Treu and S. D. Minteer, *Electroanalysis*, 2010, **22**, 757-764.

20 F. C. Macazo and S. D. Minteer, *Curr. Opin. Electrochem.*, 2017, **5**, 114-120.

21 K. Herkendell, R. Tel-Vered and A. Stemmer, *Nanoscale*, 2017, **9**, 14118-14126.

22 S. Ding, A. A. Cargill, I. L. Medintz and J. C. Claussen, *Curr. Opin. Biotechnol.*, 2015, **34**, 242-250.

23 I. Willner, E. Katz and B. Willner, *Electroanalysis*, 1997, **9**, 965-977.

24 R. A. Marcus and N. Sutin, *Biochim. Biophys. Acta, Rev. Bioenerg.*, 1985, **811**, 265-322.

25 R. Tel-Vered and I. Willner, *Isr. J. Chem.*, 2010, **50**, 321-332.

26 M. E. Yakovleva, A. Killyeni, R. Ortiz, C. Schulz, D. MacAodha, P. O. Conghaile, D. Leech, I. C. Popescu, C. Gonaus, C. K. Peterbauer and L. Gorton, *Electrochem. Commun.*, 2012, **24**, 120-122.

27 A. A. Arrocha, U. Cano-Castillo, S. A. Aguila and R. Vazquez-Duhalt, *Biosens. Bioelectron.*, 2014, **61**, 569-574.

28 Y. Hibino, S. Kawai, Y. Kitazumi, O. Shirai and K. Kano, *Electrochem. Commun.*, 2017, **77**, 112-115.

29 C. X. Cai and J. Chen, *Anal. Biochem.*, 2004, **325**, 285-292.

30 Y. Kamitaka, S. Tsujimura, N. Setoyama, T. Kajino and K. Kano, *Phys. Chem. Chem. Phys.*, 2007, **9**, 1793-1801.

31 M. Falk, Z. Blum and S. Shleev, *Electrochim. Acta*, 2012, **82**, 191-202.

32 C. Schulz, R. Kittl, R. Ludwig and L. Gorton, *ACS Catal.*, 2016, **6**, 555-563.

33 K. Sakai, Y. Sugimoto, Y. Kitazumi, O. Shirai, K. Takagi and K. Kano, *Electrochim. Acta*, 2017, **228**, 537-544.

34 J. Martinez-Ortiz, R. Flores and R. Vazquez-Duhalt, *Biosens. Bioelectron.*, 2011, **26**, 2626-2631.

35 J. Lim, N. Cirigliano, J. Wang and B. Dunn, *Phys. Chem. Chem. Phys.*, 2007, **9**, 1809-1814.

36 G. Gupta, C. Lau, V. Rajendran, F. Colon, B. Branch, D. Ivnitski and P. Atanassov, *Electrochem. Commun.*, 2011, **13**, 247-249.

37 S. Brocato, C. Lau and P. Atanassov, *Electrochim. Acta*, 2012, **61**, 44-49.

38 J. Filip and J. Tkac, *J. Biotechnol.*, 2014, **185**, S21-S22.

39 H. Q. Xia, Y. Kitazumi, O. Shirai and K. Kano, *J. Electroanal. Chem.*, 2016, **763**, 104-109.

40 S. Rubenwolf, O. Strohmeier, A. Kloke, S. Kerzenmacher, R. Zengerle and F. von Stetten, *Biosens. Bioelectron.*, 2010, **26**, 841-845.

41 C. Gutierrez-Sanchez, W. Jia, Y. Beyl, M. Pita, W. Schuhmann, A. L. De Lacey and L. Stoica, *Electrochim. Acta*, 2012, **82**, 218-223.

42 C. Adam, P. Scodeller, M. Grattieri, M. Villalba and E. J. Calvo, *Bioelectrochemistry*, 2016, **109**, 101-107.

43 Z. Q. Gao, F. Xie, M. Shariff, M. Arshad and J. Y. Ying, *Sens. Actuators, B*, 2005, **111**, 339-346.

44 T. Matsue, N. Kasai, M. Narumi, M. Nishizawa, H. Yamada and I. Uchida, *J. Electroanal. Chem. Interfacial Electrochem.*, 1991, **300**, 111-118.

45 P. O. Conghaile, D. MacAodha, B. Egan, P. Kavanagh and D. Leech, *J. Electrochem. Soc.*, 2013, **160**, G3165-G3170.

46 F. Mao, N. Mano and A. Heller, *J. Am. Chem. Soc.*, 2003, **125**, 4951-4957.

47 L. J. C. Jeuken, S. D. Connell, P. J. F. Henderson, R. B. Gennis, S. D. Evans and R. J. Bushby, *J. Am. Chem. Soc.*, 2006, **128**, 1711-1716.

48 P. Pinyou, A. Ruff, S. Poller, S. Alsaoub, S. Leimkuhler, U. Wollenberger and W. Schuhmann, *Bioelectrochemistry*, 2016, **109**, 24-30.

49 J. W. Gallaway and S. A. C. Barton, *J. Am. Chem. Soc.*, 2008, **130**, 8527-8536.

50 M. V. Pishko, A. Revzin and A. L. Simonian, *Sensors*, 2002, **2**, 79-90.

51 A. Trifonov, K. Herkendell, R. Tel-Vered, O. Yehezkeli, M. Woerner and I. Willner, *ACS Nano*, 2013, **7**, 11358-11368.

52 A. Trifonov, R. Tel-Vered, M. Fadeev and I. Willner, *Adv. Energy Mater.*, 2015, **5**, 1401853.

53 Y. Ulyanova, M. A. Arugula, M. Rasmussen, E. Pinchon, U. Lindstrom, S. Singhal and S. D. Minteer, *ACS Catal.*, 2014, **4**, 4289-4294.

54 C. Lau, M. J. Moehlenbrock, R. L. Arechederra, A. Falase, K. Garcia, R. Rincon, S. D. Minteer, S. Banta, G. Gupta, S. Babanova and P. Atanassov, *Int. J. Hydrogen Energy*, 2015, **40**, 14661-14666.

55 S. A. Neto, D. P. Hickey, R. D. Milton, A. R. De Andrade and S. D. Minteer, *Biosens. Bioelectron.*, 2015, **72**, 247-254.

56 M. Shao, M. N. Zafar, C. Sygmund, D. A. Guschin, R. Ludwig, C. K. Peterbauer, W. Schuhmann and L. Gorton, *Biosens. Bioelectron.*, 2013, **40**, 308-314.

57 Z. Zhu, F. Sun, X. Zhang and Y. H. P. Zhang, *Biosens. Bioelectron.*, 2012, **36**, 110-115.

58 S. Xu and S. D. Minteer, *ACS Catal.*, 2012, **2**, 91-94.

59 R. L. Arechederra and S. D. Minteer, *Electrochim. Acta*, 2010, **55**, 7679-7682.

60 D. P. Hickey, M. S. McCammant, F. Giroud, M. S. Sigman and S. D. Minteer, *J. Am. Chem. Soc.*, 2014, **136**, 15917-15920.

61 E. Katz and S. Minko, *Chem. Commun.*, 2015, **51**, 3493-3500.

62 P. K. Addo, R. L. Arechederra and S. D. Minteer, *Electroanalysis*, 2010, **22**, 807-812.

63 Y. H. Kim, E. Campbell, J. Yu, S. D. Minteer and S. Banta, *Angew. Chem., Int. Ed.*, 2013, **52**, 1437-1440.

64 L. Xia, K. Van Nguyen, Y. Holade, H. Han, K. Dooley, P. Atanassov, S. Banta and S. D. Minteer, *ACS Energy Lett.*, 2017, **2**, 1435-1438.

65 K. Yamamoto, T. Matsumoto, S. Shimada, T. Tanaka and A. Kondo, *New Biotechnology*, 2013, **30**, 531-535.

66 D. P. Hickey, F. Giroud, D. W. Schmidtke, D. T. Glatzhofer and S. D. Minteer, *ACS Catal.*, 2013, **3**, 2729-2737.

67 M. Frasconi, H. Boer, A. Koivula and F. Mazzei, *Electrochim. Acta*, 2010, **56**, 817-827.

68 A. Christenson, S. Shleev, N. Mano, A. Heller and L. Gorton, *Biochim. Biophys. Acta, Bioenerg.*, 2006, **1757**, 1634-1641.

69 S. Tsujimura, B. Tatsumi, J. Ogawa, S. Shimizu, K. Kano and T. Ikeda, *J. Electroanal. Chem.*, 2001, **496**, 69-75.

70 E. Katz and K. MacVittie, *Energy Environ. Sci.*, 2013, **6**, 2791-2803.

71 C. Santoro, S. Babanova, B. Erable, A. Schuler and P. Atanassov, *Bioelectrochemistry*, 2016, **108**, 1-7.

72 C. H. Jacquot, G. Lamicq, D. Salvador, S. Gounel, C. Stines-Chaumeil and N. Mano, *FEBS J.*, 2014, **281**, 240-241.

73 A. Le Goff, M. Holzinger and S. Cosnier, *Cell. Mol. Life Sci.*, 2015, **72**, 941-952.

74 S. Cosnier, A. J. Gross, A. Le Goff and M. Holzinger, *J. Power Sources*, 2016, **325**, 252-263.

75 A. Pizzariello, M. Stred'ansky and S. Miertus, *Bioelectrochemistry*, 2002, **56**, 99-105.

76 I. Willner, E. Katz, F. Patolsky and A. F. Buckmann, *J. Chem. Soc., Perkin Trans. 2*, 1998, **8**, 1817-1822.

77 C. Agnes, B. Reuillard, A. Le Goff, M. Holzinger and S. Cosnier, *Electrochem. Commun.*, 2013, **34**, 105-108.

78 F. Giroud, C. Gondran, K. Gorgy, V. Vivier and S. Cosnier, *Electrochim. Acta*, 2012, **85**, 278-282.

79 A. Ramanavicius, A. Kausaite-Minkstimiene, I. Morkvenaite-Vilkonciene, P. Genys, R. Mikhailova, T. Semashko, J. Voronovic and A. Ramanaviciene, *Chem. Eng. J.*, 2015, **264**, 165-173.

80 V. Krikstolaityte, Y. Oztekin, J. Kuliesius, A. Ramanaviciene, Z. Yazicigil, M. Ersoz, A. Okumus, A. Kausaite-Minkstimiene, Z. Kilic, A. O. Solak, A. Makaraviciute and A. Ramanavicius, *Electroanalysis*, 2013, **25**, 2677-2683.

81 M. J. Moehlenbrock and S. D. Minteer, *Chem. Soc. Rev.*, 2008, **37**, 1188-1196.

82 S. Vaddiraju, I. Tomazos, D. J. Burgess, F. C. Jain and F. Papadimitrakopoulos, *Biosens. Bioelectron.*, 2010, **25**, 1553-1565.

83 X. Y. Yang, G. Tian, N. Jiang and B. L. Su, *Energy Environ. Sci.*, 2012, **5**, 5540-5563.

84 M. J. Cooney, V. Svoboda, C. Lau, G. Martin and S. D. Minteer, *Energy Environ. Sci.*, 2008, **1**, 320-337.

85 I. Willner, Y. M. Yan, B. Willner and R. Tel-Vered, *Fuel Cells*, 2009, **9**, 7-24.

86 I. Willner and E. Katz, *Angew. Chem., Int. Ed.*, 2003, **42**, 4576-4588.

87 J. Lee, D. Lee, E. Oh, J. Kim, Y.-P. Kim, S. Jin, H.-S. Kim, Y. Hwang, J. H. Kwak, J.-G. Park, C.-H. Shin, J. Kim and T. Hyeon, *Angew. Chem.*, 2005, **117**, 7593-7598.

88 J. Wang, M. Scampicchio, R. Laocharoensuk, F. Valentini, O. González-García and J. Burdick, *J. Am. Chem. Soc.*, 2006, **128**, 4562-4563.

89 Ó. A. Loaiza, R. Laocharoensuk, J. Burdick, M. C. Rodríguez, J. M. Pingarron, M. Pedrero and J. Wang, *Angew. Chem.*, 2007, **119**, 1530-1533.

90 J. Heinze, *Angew. Chem., Int. Ed.*, 1984, **23**, 831-847.

91 K. Cammann and H. Galster, *J. Prakt. Chem./Chem.-Ztg.*, 1996, **338**, 688.

92 A. C. Fisher, "Electrochemistry Teaching Notes" in the website of the Department of Chemical Engineering and Biotechnology, University of Cambridge, 2010. http://www.ceb.cam.ac.uk/research/groups/rg-eme/teaching-notes

93 A. C. Testa and W. H. Reinmuth, *Anal. Chem. Analytical Chemistry*, 1961, **33**, 1320-1324.

94 C. Léger, S. J. Elliott, K. R. Hoke, L. J. C. Jeuken, A. K. Jones and F. A. Armstrong, *Biochemistry*, 2003, **42**, 8653-8662.

95 K. Yokoyama and Y. Kayanuma, *Anal. Chem.*, 1998, **70**, 3368-3376.

96 B. Limoges and J.-M. Savéant, *J. Electroanal. Chem.*, 2003, **549**, 61-70.

97 L. Michaelis, M. L. Menten, K. A. Johnson and R. S. Goody, *Biochemistry*, 2011, **50**, 8264-8269.

98 W. H. Freeman, in *Biochemistry*, eds. J. M. Berg, J. L. Tymoczko and L. Stryer, New York, 5 edn., 2002, ch. 8.4

99 M. H. Koo, G. Das and H. H. Yoon, *J. Nanosci. Nanotechnol.*, 2016, **16**, 3054-3057.

100 N. Yang, X. Chen, T. Ren, P. Zhang and D. Yang, *Sens. Actuators, B*, 2015, **207**, 690-715.

101 C. Yang, M. E. Denno, P. Pyakurel and B. J. Venton, *Anal. Chim. Acta*, 2015, **887**, 17-37.

102 Y. Shao, J. Wang, H. Wu, J. Liu, I. A. Aksay and Y. Lin, *Electroanalysis*, 2010, **22**, 1027-1036.

103 S. F. Oliveira, G. Bisker, N. A. Bakh, S. L. Gibbs, M. P. Landry and M. S. Strano, *Carbon*, 2015, **95**, 767-779.

104 S. Cosnier, M. Holzinger and A. Le Goff, *Frontiers Bioengin. Biotechnol.*, 2014, **2**, 45.

105 Z. Zhu, L. Garcia-Gancedo, A. J. Flewitt, H. Xie, F. Moussy and W. I. Milne, *Sensors*, 2012, **12**, 5996-6022.

106 R. Tel-Vered, O. Yehezkeli and I. Willner, *Nanobiotechnol. Biomed.* , 2012, **733**, 1-16.

107 S. D. Minteer, P. Atanassov, H. R. Luckarift and G. R. Johnson, *Mater. Today*, 2012, **15**, 166-173.

108 O. Yehezkeli, R. Tel-Vered, S. Reichlin and I. Willner, *ACS Nano*, 2011, **5**, 2385-2391.

109 A. Walcarius, *Sensors*, 2017, **17**, 1863.

110 P. N. Catalano, A. Wolosiuk, G. Soler-Illia and M. G. Bellino, *Bioelectrochemistry*, 2015, **106**, 14-21.

111 Y. Hamano, S. Tsujimura, O. Shirai and K. Kano, *Bioelectrochemistry*, 2012, **88**, 114-117.

112 K. So, Y. Kitazumi, O. Shirai and K. Kano, *J. Electroanal. Chem.*, 2016, **783**, 316-323.

113 N. Mano and L. Edembe, *Biosens. Bioelectron.*, 2013, **50**, 478-485.

114 S. Campuzano, S. A. Loaiza, M. Pedrero, F. J. M. de Villena and J. M. Pingarron, *Bioelectrochemistry*, 2004, **63**, 199-206.

115 P. N. Bartlett, V. Q. Bradford and R. G. Whitaker, *Talanta*, 1991, **38**, 57-63.

116 S. Kawai, M. Goda-Tsutsumi, T. Yakushi, K. Kano and K. Matsushita, *Appl. Environ. Microbiol.*, 2013, **79**, 1654-1660.

117 J. Chen, D. Bamper, D. T. Glatzhofer and D. W. Schmidtke, *J. Electrochem. Soc.*, 2015, **162**, F258-F264.

118 S. Kawai, T. Yakushi, K. Matsushita, Y. Kitazumi, O. Shirai and K. Kano, *Electrochem. Commun.*, 2014, **38**, 28-31.

119 K. Damar and D. O. Demirkol, *Talanta*, 2011, **87**, 67-73.

120 S. Tsujimura, A. Nishina, Y. Kamitaka and K. Kano, *Anal. Chem.*, 2009, **81**, 9383-9387.

121 M. Ameyama, E. Shinagawa, K. Matsushita and O. Adachi, *J. Bacteriol.*, 1981, **145**, 814-823.

122 S. Campuzano, R. Gaalvez, M. Pedrero, F. J. Manuel de Villena and J. M. Pingarron, *Anal. Bioanal. Chem.*, 2003, **377**, 600-607.

123 M. Bendikov, F. Wudl and D. F. Perepichka, *Chem. Rev.*, 2004, **104**, 4891-4946.

124 M. Falk, V. Andoralov, M. Silow, M. D. Toscano and S. Shleev, *Anal. Chem.*, 2013, **85**, 6342-6348.

125 A. J. Olaya, P. Ge, J. F. Gonthier, P. Pechy, C. Corminboeuf and H. H. Girault, *J. Am. Chem. Soc.*, 2011, **133**, 12115-12123.

126 S. Campuzano, V. Escamilla-Gomez, M. A. Herranz, M. Pedrero and J. M. Pingarron, *Sens. Actuators, B*, 2008, **134**, 974-980.

127 F. Giroud, D. P. Hickey, D. W. Schmidtke, D. T. Glatzhofer and S. D. Minteer, *ChemElectroChem*, 2014, **1**, 1880-1885.

128 S. Cosnier, A. J. Gross, A. Le Goff and M. Holzinger, *J. Power Sources*, 2016, **325**, 252-263.

129 M. Frasconi, G. Favero, H. Boer, A. Koivula and F. Mazzei, *Biochim. Biophys. Acta, Proteins Proteomics*, 2010, **1804**, 899-908.

130 J. A. Cracknell, T. P. McNamara, E. D. Lowe and C. F. Blanford, *Dalton T*, 2011, **40**, 6668-6675.

131 E. I. Solomon, U. M. Sundaram and T. E. Machonkin, *Chem. Rev.*, 1996, **96**, 2563-2606.

132 P. Ramírez, N. Mano, R. Andreu, T. Ruzgas, A. Heller, L. Gorton and S. Shleev, *Biochim. Biophys. Acta*, 2008, **1777**, 1364-1369.

133 B. Shoham, Y. Migron, A. Riklin, I. Willner and B. Tartakovsky, *Biosens. Bioelectron.*, 1995, **10**, 341-352.

134 J. Filip, J. Sefcovicova, P. Gemeiner and J. Tkac, *Sens. Transducers J.*, 2013, **543**, 13-17.

135 M. Pita, C. Gutierrez-Sanchez, M. D. Toscano, S. Shleev and A. L. De Lacey, *Bioelectrochemistry*, 2013, **94**, 69-74.

136 J. Vivekananthan, R. A. Rincon, V. Kuznetsov, S. Poller and W. Schuhmann, *ChemElectroChem*, 2014, **1**, 1901-1908.

137 N. Lalaoui, A. Le Goff, M. Holzinger and S. Cosnier, *Chem. - Eur. J.*, 2015, **21**, 16868-16873.

138 S. C. Barton, *Electrochim. Acta*, 2005, **50**, 2145-2153.

139 M. J. Gonzalez-Guerrero, F. J. del Campo, J. P. Esquivel, D. Leech and N. Sabate, *Biosens. Bioelectron.*, 2017, **90**, 475-480.

140 D. Pankratov, L. Ohlsson, P. Gudmundsson, S. Halak, L. Ljunggren, Z. Blum and S. Shleev, *RSC Adv.*, 2016, **6**, 70215-70220.

141 P. O. Conghaile, M. Falk, D. MacAodha, M. E. Yakovleva, C. Gonaus, C. K. Peterbauer, L. Gorton, S. Shleev and D. Leech, *Anal. Chem.*, 2016, **88**, 2156-2163.

142 M. Cadet, S. Gounel, C. Stines-Chaumeil, X. Brilland, J. Rouhana, F. Louerat and N. Mano, *Biosens. Bioelectron.*, 2016, **83**, 60-67.

143 D. Tromans, *Hydrometallurgy*, 1998, **48**, 327-342.

144 B. Chance, *J. Biol. Chem.*, 1952, **194**, 471-481.

145 C. Bourdillon, C. Demaille, J. Moiroux and J. M. Saveant, *J. Am. Chem. Soc.*, 1993, **115**, 2-10.

146 E. Katz, V. Bocharova and M. Privman, *J. Mater. Chem.*, 2012, **22**, 8171-8178.

147 J. C. He, M. Y. Huang, D. M. Wang, Z. M. Zhang and G. K. Li, *J. Pharm. Biomed. Anal.*, 2014, **101**, 84-101.

148 K. Herkendell, A. Stemmer and R. Tel-Vered, *submitted*, 2018.

149 K. Sung Kim and J.-K. Park, *Lab Chip*, 2005, **5**, 657-664.

150 A. Ranzoni, G. Sabatte, L. J. van Ijzendoorn and M. W. J. Prins, *ACS Nano*, 2012, **6**, 3134-3141.
151 M. Arruebo, R. Fernández-Pacheco, M. R. Ibarra and J. Santamaría, *Nano Today*, 2007, **2**, 22-32.
152 S. C. Tsang, C. H. Yu, X. Gao and K. Tam, *J. Phys. Chem. B*, 2006, **110**, 16914-16922.
153 H.-Y. Park, M. J. Schadt, Wang, I. I. S. Lim, P. N. Njoki, S. H. Kim, M.-Y. Jang, J. Luo and C.-J. Zhong, *Langmuir*, 2007, **23**, 9050-9056.
154 Y. Li, X. Li, J. Chu, C. Dong, J. Qi and Y. Yuan, *Environ. Pollut.*, 2010, **158**, 2317-2323.
155 T. A. P. Rocha-Santos, *TrAC, Trends Anal. Chem.*, 2014, **62**, 28-36.
156 M. Hasanzadeh, N. Shadjou and M. de la Guardia, *TrAC, Trends Anal. Chem.*, 2015, **72**, 1-9.
157 R. Hirsch, E. Katz and I. Willner, *J. Am. Chem. Soc.*, 2000, **122**, 12053-12054.
158 N. Aguilo-Aguayo, M. J. Inestrosa-Izurieta, J. Garcia-Cespedes and E. Bertran, *J. Nanosci. Nanotechnol.*, 2010, **10**, 2646-2649.
159 A. Taylor, Y. Krupskaya, S. Costa, S. Oswald, K. Krämer, S. Füssel, R. Klingeler, B. Büchner, E. Borowiak-Palen and M. P. Wirth, *J. Nanopart. Res.*, 2010, **12**, 513-519.
160 C. A. Hunter and J. K. M. Sanders, *J. Am. Chem. Soc.*, 1990, **112**, 5525-5534.
161 J. Okuda, T. Yamazaki, M. Fukasawa, N. Kakehi and K. Sode, *Anal. Lett.*, 2007, **40**, 431-440.
162 C. Liu, Z. Chen and C. Z. Li, *IEEE Trans. Nanotechnol.*, 2011, **10**, 59-62.
163 C. Liu, S. Alwarappan, Z. Chen, X. Kong and C.-Z. Li, *Biosens. Bioelectron.*, 2010, **25**, 1829-1833.
164 X. Wang, M. Falk, R. Ortiz, H. Matsumura, J. Bobacka, R. Ludwig, M. Bergelin, L. Gorton and S. Shleev, *Biosens. Bioelectron.*, 2012, **31**, 219-225.
165 M. B. Fischback, J. K. Youn, X. Zhao, P. Wang, H. G. Park, H. N. Chang, J. Kim and S. Ha, *Electroanalysis*, 2006, **18**, 2016-2022.
166 A. Ramanavicius, A. Kausaite and A. Ramanaviciene, *Biosens. Bioelectron.*, 2008, **24**, 761-766.
167 K. MacVittie, T. Conlon and E. Katz, *Bioelectrochemistry*, 2015, **106**, 28-33.
168 V. Coman, C. Vaz-Dominguez, R. Ludwig, W. Herreither, D. Haltrich, A. L. De Lacey, T. Ruzgas, L. Gorton and S. Shleev, *Phys. Chem. Chem. Phys.*, 2008, **10**, 6093-6096.
169 I. Mazurenko, K. Monsalve, P. Infossi, M.-T. Giudici-Orticoni, F. Topin, N. Mano and E. Lojou, *Energy Environ. Sci.*, 2017, **10**, 1966-1982.

170 M. Shao, M. N. Zafar, M. Falk, R. Ludwig, C. Sygmund, C. K. Peterbauer, D. A. Guschin, D. MacAodha, P. Ó Conghaile, D. Leech, M. D. Toscano, S. Shleev, W. Schuhmann and L. Gorton, *ChemPhysChem*, 2013, **14**, 2260-2269.

171 A. Ramanavicius, A. Kausaite and A. Ramanaviciene, *Biosens. Bioelectron.*, 2005, **20**, 1962-1967.

172 N. Yuhashi, M. Tomiyama, J. Okuda, S. Igarashi, K. Ikebukuro and K. Sode, *Biosens. Bioelectron.*, 2005, **20**, 2145-2150.

173 E. Katz and K. MacVittie, *Energy Environ. Sci.*, 2013, **6**, 2791-2803.

174 S. Cosnier, A. Le Goff and M. Holzinger, *Electrochem. Commun.*, 2014, **38**, 19-23.

175 X. Wei and J. Liu, *Front. Energy Power Eng.*, 2008, **2**, 1-13.

176 C. Agnes, M. Holzinger, A. Le Goff, B. Reuillard, K. Elouarzaki, S. Tingry and S. Cosnier, *Energy Environ. Sci.*, 2014, **7**, 1884-1888.

177 B. Reuillard, C. Abreu, N. Lalaoui, A. Le Goff, M. Holzinger, O. Ondel, F. Buret and S. Cosnier, *Bioelectrochemistry*, 2015, **106**, 73-76.

178 T. Miyake, M. Oike, S. Yoshino, Y. Yatagawa, K. Haneda and M. Nishizawa, *Lab Chip*, 2010, **10**, 2574-2578.

179 F. Wu, L. N. Pelster and S. D. Minteer, *Chem. Commun.*, 2015, **51**, 1244-1247.

180 M. Ameyama, E. Shinagawa, K. Matsushita and O. Adachi, *J. Bacteriol.*, 1981, **145**, 814-823.

181 K. Otsuka, T. Sugihara, Y. Tsujino, T. Osakai and E. Tamiya, *Anal. Biochem.*, 2007, **370**, 98-106.